THE HONG KONG
POLYTECHNIC UNIVERSITY
香港理工大學
Pao Yue-kong Library
包玉剛圖書館

Copyright Undertaking

This thesis is protected by copyright, with all rights reserved.

By reading and using the thesis, the reader understands and agrees to the following terms:

1. The reader will abide by the rules and legal ordinances governing copyright regarding the use of the thesis.
2. The reader will use the thesis for the purpose of research or private study only and not for distribution or further reproduction or any other purpose.
3. The reader agrees to indemnify and hold the University harmless from and against any loss, damage, cost, liability or expenses arising from copyright infringement or unauthorized usage.

IMPORTANT

If you have reasons to believe that any materials in this thesis are deemed not suitable to be distributed in this form, or a copyright owner having difficulty with the material being included in our database, please contact lbsys@polyu.edu.hk providing details. The Library will look into your claim and consider taking remedial action upon receipt of the written requests.

Pao Yue-kong Library, The Hong Kong Polytechnic University, Hung Hom, Kowloon, Hong Kong

http://www.lib.polyu.edu.hk

DECIPHERING THE ROLE OF B CELL SIGNAL-TRANSDUCING ADAPTOR PROTEIN (STAP) 1 IN THE REGULATION OF ANTIBODY PRODUCTION AND LIPID METABOLISM

DENG CHUJUN

PhD

The Hong Kong Polytechnic University

2023

The Hong Kong Polytechnic University

Department of Health Technology and Informatics

DECIPHERING THE ROLE OF B CELL SIGNAL-TRANSDUCING ADAPTOR PROTEIN (STAP) 1 IN THE REGULATION OF ANTIBODY PRODUCTION AND LIPID METABOLISM

DENG Chujun

A thesis submitted in partial fulfilment of the requirements for the degree of Doctor of Philosophy

December 2022

CERTIFICATE OF ORIGINALITY

I hereby declare that this thesis is my own work and that, to the best of my knowledge and belief, it reproduces no material previously published or written, nor material that has been accepted for the award of any other degree or diploma, except where due acknowledgment has been made in the text.

_____ (Signed)

DENG,Chujun_____ (Name of student)

Abstract

Introduction: Familial hypercholesterolemia is a common genetic disease mainly caused by the mutation of *LDLR, APOB, and PCSK9*. A fourth gene, *STAP1*, classically known to be expressed in immune cells, has been suggested to be one of the causative genes. However, the involvement of STAP1 in familial hypercholesterolemia is still controversial, as recent studies have also indicated otherwise. Despite the fact that STAP1 is mainly expressed in the spleen but dramatically increased in the liver of high-fat diet (HFD) fed mice, the pathophysiological function of STAP1 remains not known. In this study, I have systematically examined the role of STAP1 in B cell immune responses and its potential moonlighting function in immunometabolism by both loss of function and gain of function mouse models.

Methods: STAP1 global knockout (KO) mice and a recombinant adeno-associated virus (rAAV) mediated gene delivery system specifically overexpression of STAP1 in B cells were used to study the relationship between STAP1 and immunometabolism. For the immunization assay, mice were immunized with

ovalbumin as a model antigen. Antigen-specific antibody levels were assessed using ELISA. A siRNA system was employed for suppressing STAP1 in vitro. A Seahorse extracellular flux analyzer was used to measure mitochondrial respiration to determine the main function of mitochondrial-related ATP production. Flow cytometry, RT-qPCR, and Western blot analysis were performed to determine the number of mitochondria, mitochondrial function, and the expression levels of mitochondrial complexed mRNAs or proteins.

Results: Deletion of STAP1 resulted in a lower antigen-specific antibody production at mucosal sites following intranasal immunization adjuvanted with facilitated with cholera toxin in mice. Consistently, knock-down STAP1 expression in hybridoma B cells by specific siRNAs decreased the secretion of the IgG1 antibody. Mechanistically, suppression or deletion of STAP1 resulted in weaker mitochondrial respiration and glycolysis by downregulating the expression of mitochondrial biogenesis genes. In contrast, enhancing mitochondrial respiration and glycolysis were observed in primary B cells from mice with overexpressing of STAP1. In addition, increased serum cholesterol and triglyceride levels after fasting under standard chow feeding were observed in STAP1 KO mice

as compared with their wild-type littermates. While overexpressing STAP1 in B cell of HFD fed mice improved the lipid profiles.

Conclusion: In this study, I provided compelling evidence demonstrating an important role of STAP1 in immunometabolism. STAP1 is required for optimal humoral immune responses, and hence the lipid metabolism, by maintaining mitochondrial respiratory capacity in B cells. Collectively, my work has shed initial light on the elucidation of a possible link between immunity and metabolism through the expression of STAP1 in B cells. STAP1 is a novel diagnostic and therapeutic target for B cell related immunometabolic diseases.

Acknowledgments

I would like to present my sincere gratitude to all who have contributed to the completion of this thesis.

First, I present my great appreciation to my chief supervisor Dr. Wong Chi Ming. The support you gave me from the beginning of my Ph.D. study until the completion of the thesis. You are always there to help me figure out the difficulties when I encountered some barriers that I cannot go through by myself. Thank you so much indeed for all the contributions during my study. And thank you for your patience. My Ph.D. study will be less smooth without your supervision.

I would also express my special gratitude to my co-supervisor Prof Zou Xiang. You always provide ideas and help me to go back to the right way to solve the problem. It is my first-time studying immunology; I remembered your encouragement to help me grow up in my Ph.D. journey.

I am thankful for the suggestions from all the members of the Depart of Health Technology and Informatics, PolyU. Especially, I want to thank Prof Yip Shea-ping, Prof Ying, Tin Cheung Michael, Prof Leung Hang Mei Polly, Prof ZHANG Weixiong, Dr. CHENG King Yip Kenneth, Dr. HUANG Chien-ling, Dr. LAW Ka

Wai Helen, Dr. Ma Chun Hang Alvin, Dr. SIU Kit Hang Gilman, Dr. CHEN Xiangyan Fiona, Dr. LIN Liang-ting, Dr. TSE Kai Hei Fanki, Dr. YOO Jung Sun, Dr. CAI Yin David, and Dr. TAM Shing Yau Macro.

My thanks also go to Dr. Hui Raymond, Ms. LI Karen, Ms. LI Maple, and Ms. MENG Ivy Xiangyu, Health Technology, and Informatics; Dr. CHOW Ho-yin Ryan and Dr. Li Wai-sum Rachel for offering all the technical training and support for the instruments. And I also offer my admiration to Dr. Au LAI Shan Alice, Mr. TANG Wang Him Vincent, and Mr. HO Hei Man, Centralised Animal Facilities, PolyU, for all the mouse work management.

I am grateful to my groupmates Dr. YEUNG Ho Yin Martin, Ms. CHAN Ka Ying, Mr. LI Xiang, Ms. WU Mengyao, Mr. Lo Tak Ho, and Dr. WONG Alex Ngai Nick for all kinds of support to help me complete the thesis. I would also extend my thanks to all the groupmates of Prof Zou Xiang, Arka, Eden, Yuxuan, and Olifan for their support of my big-scale experiments.

I wish to thank all my colleagues for being around the lab to always standing by me, Chenxi, Yao, Jenny, Kent, KK, Huige, Kelvin, MJ, Xiaofan, Becca, Liyue, and Mohan.

At last, I want to present my heartful appreciation to my family, my best friend LEUNG Ka Kei Yuki, C.C.C, and my lovely Air. Without any one of you, I believe I will not achieve here.

The table of contents

The list of figures

Chapter 1- Introduction

1 Introduction

1.1 Immunology

The immune system is a complex network depending on cells and proteins, protecting the body from infections, such as germs, fungi, and viruses. The main components of the immune system in our body are white blood cells, antibodies, complement system, lymphatic system, spleen, bone marrow, and thymus. The immune system divides into innate immunity and adaptive immunity. The natural immune system provides immediate protection against some known infections [1-2]. In contrast, the adaptive immune system creates immune cells, B and T lymphocytes, to construct a more complex defence system for resisting imprecise defences. Furthermore, the dendritic cell (DC) processes and presents microbial antigens to lymphocytes and provides them with signals to link the innate immune system and the adaptive immune system. Ensuring the interaction of these two immune systems can protect our body from all kinds of infections well[3].

Cellular immunity and humoral immunity compose human adaptive immunity. T cells in cellular immunity can activate the B cell of humoral immunity for proliferation and differentiation. And antibodies will be produced in plasma cells finally. The vaccination, vaccine acts as an antigen to activate our immune

response in our body. Briefly, when the antigen, for example, bacteria, gets into our bodies, they will first encounter the antigen-presenting cell (APC), especially the dendritic cell (DC). Next, they will be phagocytosed into small fragments and presented to the Naïve T cell by DC. Currently, antigen fragments act as stimulatory to activate naïve T cell differentiation. The Naïve T cell will differentiate into two different T helper (Th) cells based on the different antigens. Th1 and Th2 cells. Finally, the Th cell activates B cell differentiation and plasma B cell to secrete antibodies.

During the vaccination process, the antigen is primarily captured by DC and presented to a naïve T cell by DC. Various Th cells activation were induced by the diverse source of antigen, and the polarization of Th1 and Th2 cells is proposed to be built on cytokines selection. Th1 cell identifies the endogenous antigen, for example, bacteria, protozoa, and fungi producing interferon-gamma (IFN-γ), then promotes the B cell class-switch in the germinal centre to secrete IgG2a or iGg2c. However, the Th2 cell recognizes exogenous antigens, like helminths, secreting interleukin (IL)-4, IL-12, and IL-5, which motivate class-switch production of IgG1[4-6].

After Th cell activation, it induces B cell differentiation and migration to the B cell zone in secondary immune tissue to form a germinal centre. In the germinal centre, B cell improves their antibody affinity after somatic hypermutation (SHM). B cell with high affinity-antibodies production capacity is selected to develop into plasma cell or memory cell. At the same time, another B cell with low or no power is abolished[7]. Intriguingly, related to metabolism, germinal centre B cells rely on fatty acid oxidation to provide energy for proliferation[8]. Moreover, it is reported that hypercholesterolemia impairs immunity in Tuberculosis[9] and Atherosclerosis[10].

1.2 Vaccination

Vaccination is a highly effective and sustainable strategy for preventing and combating disease-causing pathogens such as bacteria and viruses that affect human health [11]. Vaccines work by priming our immune system to recognize these pathogens in advance by simulating an infection. This type of "infection" can induce our immune system to produce T-lymphocytes and antibodies. When our body is attacked by similar pathogens in the future, our immune system can recognize the invading pathogens and launch efficient adaptive immune responses to remove them.

However, the performance of vaccines can vary significantly between individuals in terms of both safety and efficacy. Some individuals may experience a strong reaction from the vaccine; for example, around 0.2% of individuals who receive full COVID-19 vaccination may experience allergic reactions or anaphylaxis [12]. Additionally, approximately 2-10% of healthy people fail to produce expected levels of antibodies in response to routine vaccines within a reasonable timeframe [13]. This heterogeneity in immunogenicity is often not considered when assessing disease control measures. As a result, it is crucial to address basic questions about vaccination, such as identifying individuals at risk for poor immunogenicity and/or serious adverse events after vaccination, determining the appropriate dosage and frequency of vaccine doses needed to fully protect an individual, and exploring any immunogenetic factors associated with host responses to vaccination.

The literature reports that various factors, including age and gender, can be associated with differences in immune responses to vaccines. For instance, females and younger participants appear to have an increased capacity to mount humoral immune responses to the SARS-CoV-2 BNT162b2 vaccine [14]. There is growing interest in understanding the genetic influence of predetermined factors, such as

gene expression levels and polymorphisms, on vaccine effects at both the individual and population levels.

1.3 Immunometabolism

Energy and metabolism building are needed for all living cells or organisms. The booming research of immunometabolism provides more information to understand how metabolic resources maintain adaptive and innate immune responses. More and more evidence prove that the interaction between metabolism and immune responses regulates cells' function. Primary studies indicate that inflammatory cytokines, which increase in obese adipose tissue, cause metabolic disease[15]. Moreover, activated germinal centre B cells that requires fatty acid oxidation and glycolysis to generate energy to support their antibodies-producing function[16-17]. That is to say, the dysfunction of metabolic processes in immune cells may trigger many human diseases such as diabetes, obesity, and sepsis [18].

In the immune system, B cells play a crucial role in the immune response through their ability to produce antibodies. As mentioned above, it is reported that energy generation was vital for germinal centre B cells to secrete antibodies, immunoglobulin class switching, and their normal function maintenance.

I reviewed the literature as well as various databases and found that the expression of an immune cell-specific gene called Signal Transducing Adaptor Family Member 1 (STAP1; also known as BCR downstream signalling 1 [BRDG1]) is highly associated with pre-existing immunity towards various vaccines' performance. The evidence includes: (1) after various infections, such as COVID-19 and influenza, the expression level of STAP1 mRNA in peripheral blood increased dramatically [19-21]; (2) according to a five-year study analysing the correlation of antibody and B cell responses to the influenza vaccine in younger and aged individuals [22], the expression of many B cell signalling genes (including STAP1) are higher in younger but not aged subjects; and (3) In general, females induce stronger immune functions and higher antibody levels, composed of more functional antibodies, but also experience more adverse reactions to vaccination [23]. Based on a study of sex differences in immune responses to the seasonal influenza vaccination [24], females have higher levels of influenza A-specific memory B cells than males after vaccination. The authors found that, STAP1 is one of the sex-differential expressed gene are more highly expressed in females relative to males, indicating the heightened activity of females' B cells after vaccination relative to those of males.

Interestingly, STAP1 was reported to be one of genes associated with familial hypercholesterolemia (FH) since 2014 [25-27]. Although the hypercholesterolemia phenotype of STAP1 mutation carriers is milder than those well-known FH causative genes such as LDLR, APOB, and PCSK9. STAP1 mutation carriers showed significantly higher levels of plasma total cholesterol and LDL compared with non-affected relatives and have a very slightly but significantly higher triglyceride levels [25-27].

1.4 Familial Hypercholesterolemia (FH)

Familiar hypercholesterolemia is a common genetic disease with an estimated prevalence range between 1:500 to 1:250. Elevated plasma low-density lipoprotein cholesterol (LDL-C) is the clinical diagnosis of hypercholesterolemia. Classic FH is caused by a defect in the *LDLR*, while a functionally similar effect is caused by mutations in *APOB* or *PCSK9* [28-30]. Proteins produced from these three genes are essential for the normal function of *LDLR*. Mutations in any of these three genes prevent cells from making functional receptors or changing the receptors' function. The *LDLR* gene provides signals for making a protein, a low-density lipoprotein receptor (LDLR). This type of receptor binds to low-density lipoprotein (LDLs)

particles, the primary carriers of cholesterol in the blood. By removing LDLs from the bloodstream, these receptors play a vital role in regulating cholesterol levels. Some *LDLR* gene mutations reduce producing the amount of LDLR protein, decreasing the binding to LDL particles, which prevents it removing excessive LDLs from blood. Other mutations disrupt the LDL receptor's ability to remove LDLs from the bloodstream. For example, mutation of the *APOB* gene will increase a higher expression level of APOB protein, which stops LDLR binging to LDL particle, resulting from APOB protein acts as a ligand for LDL. The principle of *PCSK9* gene mutation is the same as the *APOB* gene. PCSK9 protein degrades the LDL receptors. As a result, people with mutations in these three genes have very high blood cholesterol levels, and it is deposited abnormally in tissue[29, 31-32].

To understand this genetic mechanism in more thorough detail, researchers found more and more genes by sequencing analysis. But the relationship between FH and these genes still needs time to be investigated. Among these newly discovered genes, STAP1 was classified as the fourth gene in[30] [26] FH. But it is still subject to controversy.

1.5 Role of B lymphocytes in non-alcoholic fatty liver disease

Non-alcoholic fatty liver disease (NAFLD) and its associated complications are developing into one of the most important health problems internationally. The liver served as both a metabolic and an immune organ. The crosstalk between hepatocytes and intrahepatic immune cells acts a key role in coordinating a dual function of the liver in terms of the defence of the host from antigenic overload because of getting nutrients and gut microbiota antigenic stimulation through facilitating immunologic tolerance. B cells are the most abundant lymphocytes in the liver. The essential role of intrahepatic B cells in energy metabolism under different immune conditions is now emerging. The accumulating evidence has demonstrated that the antibodies and cytokines produced by B cells in the microenvironment play key and distinct roles in the pathogenesis of NAFLD. For example, the cytokines produced by B cells may play an important role in the production of different phenotypes. The studies conclude that NAFLD is aggravated by pathogenic antibodies but alleviated by cytokines secreted by B cells [33].

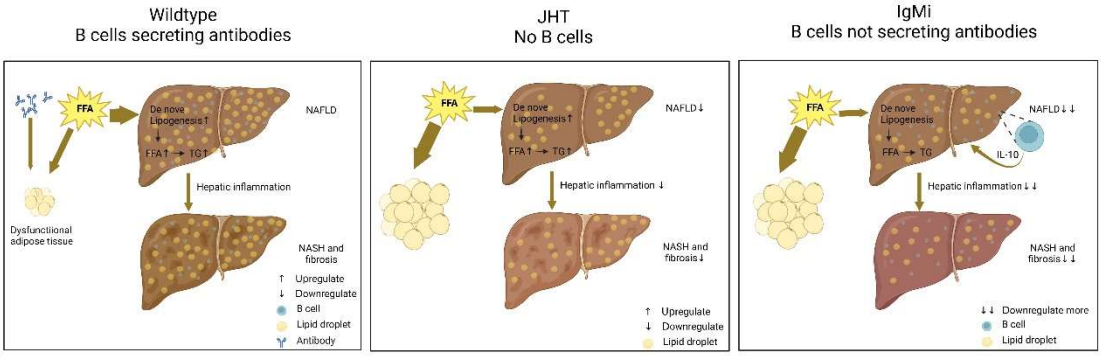

Figure 1.3.1 B cells have both detrimental and protective effects in diet-induced NAFLD.

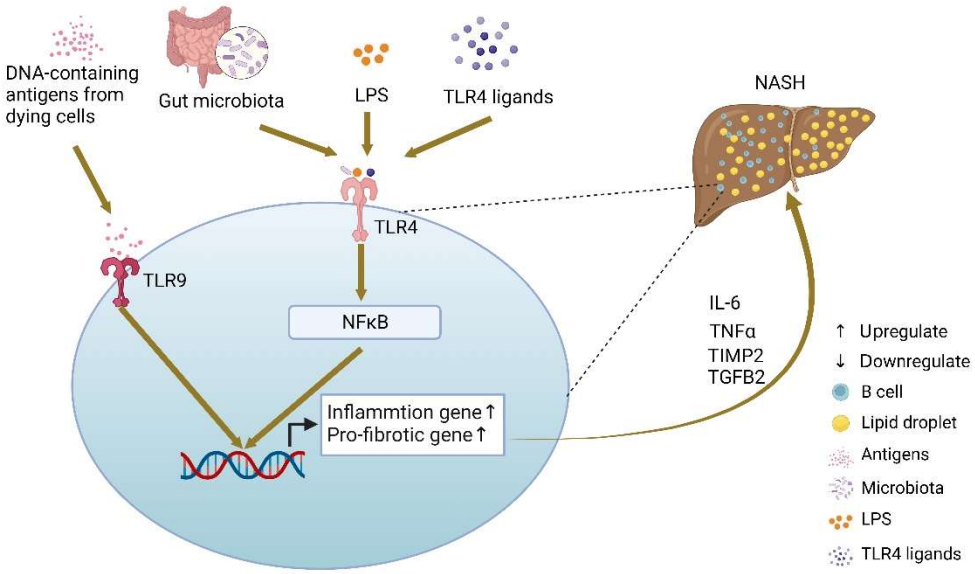

Figure 1.3.2 The proposed mechanism of activation of intrahepatic B cells during the disease progression of NASH.

1.6 Signalling transducing adaptor protein 1 (STAP1)

Signalling transducing adaptor protein 1 (STAP1), also known as B-cell antigen receptor downstream signalling 1 protein (BRDG1), is expressed highly in immune tissues, including bone marrow, thymus, spleen, appendix, and lymph nodes[34-36], and particularity expresses in B cells refers to the Human atlas database[37]. STAP1 is located on chromosomal region 4q13.2 with 10 exons, composed of a Pleckstrin homology domain, the Src homology 2 (SH2) domain, and several tyrosine phosphorylation sites[38]. Recently, STAP1 is investigated as the fourth causative gene of hypercholesterolemia from 2014. Fouchier and colleagues found that STAP1 variant carriers (n=40) had significantly higher plasma total cholesterol and LDL-C levels compared with non-variants carriers (n=91)[26]. He first connected STAP1 with FH and named it as familiar hypercholesterolemia fourth (FH4). Three main STAP1 variants were found in STAP1 carriers, p. Leu69Ser, p. Il271Thr, and p. Glu97Asp in their study. Besides, other STAP1 variants were implicated in FH by the PolyPhen-1 prediction model or genetic test[25, 27, 39-40]. On the contrary, more and more researchers point out that STAP1 variants has no association with FH by clinical data analysis and lipid trait[41-43].

Except for the variant's analysis, Loaiza and colleagues validated whether STAP1 was involved in FH using global STAP1 knockout (KO) mice and their wildtype (WT) littermates [44]. In this study, they postulated that the STAP1 expressed in immune cells-controlled LDL homeostasis to affect hepatic function. They measured the general lipid parameter of 39 STAP1 variants (proposed by Fouchier [26]) and 71 family control in a clinal study. They monitored the plasma lipid level and general characteristics before and after the western diet (42% kcal) for 2 weeks and 4 weeks, using a whole body STAP1-KO mouse model, compared with their corresponding wild type littermates. HepG2 cells were coculture with peripheral blood myonuclear cells isolated from patients with STAP1 variants and control. mRNA and protein level of LDLR and LDL uptake was measured after coculture. They also checked the B cells population in peripheral blood myonuclear cells from patients with STAP1 variants, compared with the control. Surprisedly, there is no change on the frequencies of B cell among the patients and healthy individuals[26].

Interestingly, they could not find any difference in all assays between STAP1 variants and control groups, even the B cells population. They concluded that STAP1 should be excluded from the targeted sequencing panel of FH. Followed by Kanuri and colleagues, also recruited global STAP1-KO mice, feeding with a

16-week western diet, a longer time than Loaiza[45], as they considered a 16-week western diet was sufficient according to previous publishes. They performed a similar experiment as Loaiza did, and similarity their results also presented no changes between STAP1-WT and STAP1-KO groups. Unlike Loaiza, they investigated the population of the subtype of B cells and IgG in STAP1-KO mice but still found no difference.

Kanuri indicated that these two experiments focused on using STAP1-KO mice, which were regarded as a loss of function model, and could not get any hints from a gain of function variants in STAP1. That means the missense mutation on STAP1 might translate into another potential functional protein to break the balance in hepatic homeostasis. Therefore, I propose to confirm whether STAP1 is needed for maintaining hepatic homeostasis.

To further explore the connection between STAP1 and FH, in this study, the phenotype of STAP-KO mice under standard chow (STC) feeding was measured, and the role of STAP1 in FH would be clarified using overexpression in wild type STAP1 model via Adeni-associated viruses (AAV) system with B cell specific promoter, which differs from other models used previously.

It is worth noting that STAP1 is mainly observed in immune cells. As mentioned before, some researchers check the population of immune cells, primarily B cells, to find some clues for better understanding. But they discover that STAP1 deficiency does not affect the population of B cells, the subtype of B cell, and IgG[44-45].STAP1 is known as the direct substrate of Tec, which is related to the intracellular signaling mechanism of cytokine receptors, lymphocytes surface antigens, and integrin molecules, playing significant roles in the immune system by regulating immune functions[35-36, 46]. Also, researchers are shifting from metabolism to immunity. Lately, studies release that STAP1 does not impact the phosphorylation levels of marker protein involved in pre-BCR signaling and CREB or other pathways, PI3K, Ras, JNK, p38, NFκB, which primarily mediated proliferation and survival of cells [47]. Recently, it is reported that STAP1 acts a key role in mediating chronic myeloid leukemia (CML) stem cell survival by increasing the anti-apoptotic gene expression via improving the activity of STAT5, suggesting the direct collaboration between STAP1, STAT5, and BCR—ABL in CML cells[48-49].

Table 1.1 The Summary of Human STAP1 Variants Found in Different Studies

This table provides a list of STAP1 SNPs with information about the respective changes and association with FH.

SNPs	Nucleotide	Amino acid change	Domain (position)	Associated with FH	References
rs141647540	c.35G> A	p.Arg12His		No	[41]
				No	[50]
				No	[51]
rs201996284	c.-60A > G	NA		No	[52]
				No	[50]
				No	[51]
rs79388522	c.139A> G	p. Thr47Ala	Pleckstrin homology domain (25-121)	Yes	[53]
rs938523789	c.206T > C	p. Leu69Ser		Yes	[26]
rs141647940	c.212T > C	p. Ile71Thr		Yes	[26]
rs199787258	c.291G > C	p. Glu97Asp		Yes	[26]
				Yes	[51]
				No	[50]
rs14983575	c.414G> C	No changes		No	[41]
rs199787258	c.526C > T	p. Pro176Ser		Yes	[54]
				No	[41]
				No	[50]
rs146545610	c.619G > A	p. Asp207Asn	Src homology 2 domain (177-280)	Yes	[26]
				No	[41]
				No	[52]
rs12948217	c.693C> T	No changes		No	[51]
-	c.803T > C	p. Ile268Thr		No	[52]

Furthermore, STAP1 regulates chronic myeloid leukemic stem cells by suppressing apoptosis through the adjustment of STAT5[48]. In invariant natural killer T (iNKT) cells, STAP1 is proposed to regulate Con A-induced signals, which is still needed to be clarified in molecular mechanism[55]. In studies published last year, STAP1 is indicated to interact with mast cells resting and naïve B cells by database analysis[48]. Moreover, STAP1 is listed as one of the ten top differentially expressed genes in COVID-19 patients' lungs relying on sequencing data, compared with healthy people[56]. Together, the function of STAP1 in immunity is also important to clarify.

Based on the above observations, we hypothesized the B cell STAP1 may plays an important role in linking inflammation and lipid metabolism. In this study, we used both loss- and gain-of-function experiments in mouse and cell models to explore the role of STAP1 in B cell in vaccination and metabolism reprogramming. As mouse and human STAP1 proteins share 83% identity and 90% similarity and the regions for key domains are almost the same, we believe the function and role of STAP1 in antibody production by our mouse model could be extrapolated humans.

Chapter 2- Materials and methods

2 Materials and methods

2.1 Materials

2.1.1 Chemical and reagents

Reagents	Provider	Catalog number
Direct PCR lysis reagent (Tail)	Viagen, USA	102-T
Dulbecco's modified eagle medium, powder, high glucose, pyruvate	Thermofisher, USA	12800082
Fetal Bovine Serum, qualified, Brazil	Thermofisher, USA	10270106
Penicillin-Streptomycin (10,000 U/mL)	Thermofisher, USA	15140163
Hanks' Balanced Salt Solution, calcium, magnesium	Thermofisher, USA	14025076
TRIzol™ Reagent	Thermofisher, USA	15596018
PageRuler™ Plus Prestained Protein Ladder, 10 to 250kDa	Thermofisher, USA	26620

TEMED	Thermofisher, USA	17919
Collagenase, Type II, powder	Thermofisher, USA	17101015
Ethidium Bromide Solution	Thermofisher, USA	17898
SYBR™ Safe DNA Gel Stain	Thermofisher, USA	S33102
Pierce™ TMB Substrate Kit	Thermofisher, USA	34021
Richard-Allan Scientific™ Neutral Buffered Formalin (10%)	Thermofisher, USA	5705
Richard-Allan Scientific™ Histoplast Paraffin	Thermofisher, USA	8330
Lipofectamine™ 2000 Transfection Reagent	Thermofisher, USA	L3000001
Trypan Blue Stain (0.4%)	Thermofisher, USA	T10282
2×Es Taq MasterMix	CoWin Biosciences, China	CW0690

ChamQ SYBR Color qPCR Master Mix	Vazyme,China	Q41-02
RevertAid RT Reverse Transcription Kit	Thermofisher, USA	K1691
Insulin, Human Recombinant	Sigma-Aldrich, USA	91077C
Bovine serum albumin	Sigma-Aldrich, USA	05470
Proteinase K from Tritirachium album	Sigma-Aldrich, USA	P2308
D-(+)-Glucose	Sigma-Aldrich, USA	346351
Sodium pyruvate	Sigma-Aldrich, USA	P3662
Sodium chloride	Sigma-Aldrich, USA	S9888
Sodium bicarbonate	Sigma-Aldrich, USA	S5761
30% Acrylamide/Bis Solution, 37.5:1	Bio-Rad, USA	1610158
Immun-Blot PVDF Membrane	Bio-Rad, USA	1620177
Medical X-ray film	Fuji, Japan	Super HRU30
Protease Inhibitor Cocktail	MedChemExpress, USA	HY-K0010

2-Mercaptoethanol	Bio-Rad, USA	1610710
Clarity Western ECL Substrate	Bio-Rad, USA	1705061
Clarity Max Western ECL Substrate	Bio-Rad, USA	1705062
Concanavalin A	Sigma-Aldrich, USA	
LPS	Sigma-Aldrich, USA	L2654
Flt3-L	PeproTech	250-31L
human TGF-β	R&D System	240-B-002/CF
IL-5	R&D System	405-ML-005/CF
oligomycin	Cayman Chemical	11341-10MG
FCCP	Cayman Chemical	15218-50MG
2-DG	Sigma-Aldrich, USA	SMB00932
Rotenone	Cayman Chemical	13995-5G
Antimycin	Sigma-Aldrich, USA	A8674-50MG
Cholera toxin	List Biological Labs, USA	100B
S100A4	Gentaur Molecular Products, Belgium	01-2081A4M

2.1.2 Biochemical assay

Assay	Provider	Catalog number
Pierce™ BCA Protein Assay Kit	Thermofisher, USA	23225
Mito Green Tracker	Thermofisher, USA	M46750
Mito Red Tracker	Thermofisher, USA	M46752
Mito Sox	Thermofisher, USA	M36008
Cholesterol measurement kit	Solarbio, China	BC0625
Triglyceride measurement kit	Solarbio, China	BC1980
LDL-C measurement kit	Sino, China	
HDL-C measurement kit	Sino, China	CN107449748B
EasySep™ Mouse CD11c positive selection kit	STEMCELL, Canada	#18780
EasySep™ Mouse F4/80 positive selection kit	STEMCELL, Canada	#100-0659
EasySep™ Mouse CD19 negative selection kit	STEMCELL, Canada	#19814

EasySep™ Mouse CD3 negative selection kit	STEMCELL, Canada	#19851
Mouse anti-IgA	Thermofisher, USA	88-50450-88

2.1.3 Primer sequence

Primer name	Forward (5'-3')	Reverse (5'-3')
Mouse-*HPRT*	CCCCAAAATGGTTAAGGTTGC	AACAAAGTCTGGCCTGTATCC
Mouse-*GAPDH*	AGGTCGGTGTGAACGGATTTG	TGTAGACCATGTAGTTGAGGTCA
Mouse-*β-actin*	ACCTTCTACAATGAGCTGCG	CTGGATGGCTACGTACATGG
Mouse-STAP1	GAGAAAGAGAAGGAGCCAGTAC	GCCTCAGGATCATATTTCCCC
Mouse-*CD19*	GAGAAGGAAAAGGAAGCGAATG	AGAGGTAGATGTAGGAAGGGAG
Mouse-*CD3*	TGGAGCAAGAATAGGAAGGC	CATAGTCTGGGTTGGGAACAG
Mouse-*CD11c*	TTCAAGGAGACAAAGACCCG	AGAGAAAAGTTGAGGCGAAGAG
Mouse-F4/80	ACCACAATACCTACATGCACC	AAGCAGGCGAGGAAAAGATAG
Mouse-*goblin*	GAAGCGATTCTAGGGAGCAG	GGAGCAGCGATTCTGAGTAGA

Mouse-*COXIII*	CGTGAAGGAACCTACCAAGG	ATTCCTGTTGGAGGTCAGCA
Mouse-*TFAM*	CCTTCGATTTTCCACAGAACA	GCTCACAGCTTCTTTGTATGCTT
Mouse-*CYTB*	CCCTAGCAATCGTTCACCTC	TCTGGGTCTCCTAGTATGTCTGG
Mouse-STAP1(genotyping)	GAGAACAACGAAACTAACATGAAGAGC	TGTGAGCTAAGTAGCAACCAATCT
		TCGTGGTATCGTTATGCGCC
Mouse-*MTND5*	ACCAGCATTCCAGTCCTCAC	ATGGGTGTAATGCGGTGAAT
Mouse-*NRF1*	GCACCTTTGGAGAATGTGGT	GGGTCATTTTGTCCACAGAGA
Mouse-*COX //*	TTTTCAGGCTTCACCCTAGATGA	GAAGAATGTTATGTTTACTCCTACGA ATATG
Human-HPRT	TGCTGAGGATTTGGAAAGGG	ACAGAGGGCTACAATGTGATG
Human-STAP1-1	GTAGACCTCACATGCCTTACTG	CTCTCCATTCTTCCCCACTTTC

Human-STAP1-2	AATTCACCCTTGTTTTGCCG	AGGTAGGAGTGACACGTTTTG
Human-STAP1-3	ACCTGTAACACTCCCAAACC	CTTCAACTTTTCACTTCTCCCTTC

2.1.4 Buffers

Medium and buffer	Recipe
Complete growth DMEM	DMEM supplemented with 10% fetal bovine serum (FBS) and 1% penicillin and streptomycin (PS)
Phosphate buffered saline (PBS)	137 mM NaCl, 2.7 mM KCl, 4.3 mM Na2HPO4, 1.4 KH2PO4 (pH 7.4)
Radioimmunoprecipitation (RIPA) buffer	150 mM NaCl, 50 mM Tris HCl, 2 mM EDTA, 0.1% SDS, 1% NP-40 (pH 7.4)
Sodium citrate buffer	0.1 mol/L sodium citrate, 0.1% Tween 20, pH 6.0
Tris-Acetate EDTA (TAE)	40 mM Tris-acetate, 2 mM EDTA, pH 8.0
SDS-PAGE running buffer	25 mM Tris, 192 mM glycine, 0.1% SDS (pH 8.3)
Transfer buffer	25 mM Tris, 192 mM glycine (pH 8.3)
Tris-buffered saline, 0.1% Tween 20 (TBST)	20 mM Tris, 150 mM NaCl, (pH 7.6)

5X SDS loading dye	250 mM Tris-Cl (pH 6.8), 0.05% Bromophenol blue, 50% Glycerol, 10% SDS, 5% 2-Mercaptoethanol
Stripping buffer	62.5 mM Tris-Cl (pH 6.7), 2 % SDS, 100 mM βmercaptoethanol
ELISA washing buffer	PBS with 0.01% Tween 20
ELISA reagent diluent	1% BSA in 1x PBS (0.22 μm filtered)
Phosphate-buffered saline, 0.1% Tween 20 (PBST)	PBS with 0.1% Tween 20
FACS	5 mM EDTA, 50 Mm HEPS, 1% BSA

2.1.5 Antibodies

Antibodies	Provider and catalog number	Usage and Dilution factor
Anti-STAP1	Abcam; ab103646	WB (1:1000)
Anti-PHB	Abcam; ab224635	WB (1:1000)
Anti-β-actin	#sc-47778, Santa Cruz	WB (1:5000)
Total OXPHOS Rodent WB antibody cocktail	Abcam; ab110413	WB (1:2000)
Anti-CD19	BD Biosciences; 561743	Flow cytometry
Anti-CD45	Life Technologies-eBioscience™; 11-0452-85	Flow cytometry
Anti-B220	BD Biosciences; 558108	Flow cytometry
Anti-CD138	BD Biosciences; 563192	Flow cytometry
Anti-IgA	Southern Biotech; 1040-05	ELISA (1:2000)
Anti-IgG	Southern Biotech; 1030-05	ELISA (1:4000)

Anti-IgG2c	Southern Biotech; 1079-05	ELISA (1:4000)
Anti-IgG1	Southern Biotech; 1070-05	ELISA (1:4000)
Anti-CD3	Bio-gene; 564008	Flow cytometry
Anti-MHC- II	Life Technologies-eBioscience™; 17-5320-82	Flow cytometry
Anti-CD11c	Life Technologies-eBioscience™; 12-0114-83	Flow cytometry
Anti-CD80	BD iosciences; 560526	Flow cytometry
Anti-CD86	Life Technologies-eBioscience™; 11-0862-85	Flow cytometry

2.1.6 Diets

Diets	Provider	Catalog number
Rodent Diet With 45 kcal% Fat	Research Diets	D14251

2.2 Method

2.2.1 Global STAP1 knockout mice and diet

The STAP1-KO mice were given by Professor Xu's group at Hong Kong University. Briefly, STAP1-KO mice on C57BL/6N background were generated by a refined strategy for conditional gene inactivation, developed that relies on the DNA recombinase Cre and its recognition (loxP) sites. For conditional mutagenesis, the target gene STAP1 is modified by inserting two loxP sites that enable the excise of the flanked (floxed) STAP1 exon 5 through Cre-mediated recombination. Conditional mutant mice are obtained by crossing the floxed strain with a Cre transgenic line such that the target gene becomes inactivated in vivo within the expression domain of Cre. Heterozygous STAP1 ($STAP1^{+/-}$) C57BL/6N mice were used for brother-sister mating and generated homozygous wildtype ($STAP1^{+/+}$) mice and corresponding knockout ($STAP1^{-/-}$) littermates. To assess the genotype of every mouse before engaging in experiments, ear snip genotyping was conducted and PCR products of 252bp and 136bp correspond $STAP1^{+/+}$ and $STAP1^{-/-}$ respectively. Mice were fed with a standard chow diet (STC) with 12 hours of light and dark cycles. 8-week-old male and female mice were applied for lipid and glucose metabolism measurement.

2.2.2 STAP1 overexpressed mice

The AAV-mB19-mSTAP1 plasmid was purchased from the company. For the AAV virus purification, the plasmid was co-transfected with AAV-MCS (targeted explicitly to the B cell), and AAV-Pxx6 (helper gene but lacking adeno structural and replication) and AAV-DJ at a ratio of 1:1:1 in HEK293 cells, and the medium was collected after two-day transfection. AAV-MSC plasmid was used by the corresponding control. Purification was performed, followed by a previously published reference. 8 weeks after intraperitoneal injection, mice could be recruited into experiments.

2.2.3 Glucose metabolism

Feeding glucose was measured randomly while fasting glucose was measured after 16 hours of fasting. After baseline serum glucose measurement, various drug was injected for several tolerance tests. For the glucose tolerance test (GTT), blood glucose was measured at time point 15, 30, 45, 60, 90, and 120 minutes after intraperitoneal 2g/kg glucose injection. For the insulin tolerance test (ITT) and pyruvate tolerance (PTT), 0.5U /kg insulin and 2g/kg pyruvate intraperitoneal

injection were administered, respectively, and blood glucose levels were detected at the same time point.

2.2.4 Lipid measurement

Serum total cholesterol was estimated using a Total cholesterol level measurement kit (Solarbio, BC0625), and serum triglyceride was measured using a Total cholesterol level measurement kit (Solarbio, BC1980) following manufacturer instructions. LDL-C and HDL-C were determined by the LDL-C measurement kit (BIOSINO BIO-TECHNOLOGY AND SCIENCE INC, YS73-76) and HDL-C measurement kit (BIOSINO BIO-TECHNOLOGY AND SCIENCE INC, YS69-72), separately.

2.2.5 Cell preparation

For single cell isolation from spleen and bone marrow, STAP1-WT and STAP1-KO mice were sacrificed after anesthetizing by isoflurane. Spleen, Tibia, and femur were collected for isolation. To harvest single cells from the spleen, crushing the total spleen above the cell strainer, followed by flushing the filter with RPMI-1640

medium containing 10%FBS to collect the cells. Seed the with the density of 10^6/ml after red blood cell lysis. For single cells from bone marrow, Tibia and femur were cut by the end of the bone, flushing the cavity with a culture medium. Cells could be harvested after red blood cell lysis.

2.2.6 Flow cytometry

After cell preparation, cells were washed with FACS twice and resuspended with the antibodies diluted in FACS (5 mM EDTA, 50 Mm HEPS, 1% BSA). For cell surface markers staining, corresponding antibodies were diluted in the FACS buffer, and incubated with the cells for 30 minutes on ice, protected from light. For intracellular markers, Foxp3/Transcription Factor staining buffer was used refer to the information sheet (Thermo; 00-5523).

2.2.7 RNA extraction, reverse transcription, and Quantitative reverse transcription PCR (RT- qPCR)

Total RNA was extracted from cells or tissue collected from mice according to the guanidinium thiocyanate-phenol-chloroform method. 1 μg RNA was used to transcript into cDNA using a Reverse Transcriptase M-MLV kit (Takara, 2640A). qPCR was performed using ChamQ SYBR Color qPCR Master Mix (Vazyme, Q41-02).

2.2.8 Western blot

The total cell lysate was harvested after cell collection by trypsinized and centrifuged after 13000g, 15 minutes from the supernatant. The lysate was normalized at the same protein concentration by BCA protein concentration assay before western blot. The total cell lysate was resolved on SDS-PAGE and transferred to a polyvinylidene difluoride transfer membrane (Bio-Rad, USA). The filters were then immunoblotted with each Ab. Immunoreactive proteins were visualized using an ECL detection system (Bio-Rad, USA) and captured by a Bio-Rad Chemidoc Imaging System.

2.2.9 Immunization

STAP1-WT and STAP1-KO mice were divided into four groups respectively in this immunization assay, naïve, Ovalbumin (OVA) (Sigma-Aldrich, A5503), and OVA with adjuvant. OVA is generally used as an experimental vaccine antigen in immunization. In the OVA group, the mouse was intranasally immunized with 10μg OVA each. In this study, S100A4 and Cholera Toxin (CT) were used as the adjuvants promoting the immune response and mixed with OVA for intranasal injection at a dose of 10μg and 1μg per mouse. Besides, no treatment was presented in the naïve group.

For immunization, mice were anesthetized with isoflurane and getting immunized with antigen with or without adjuvant by pipetting the liquid into the mice's nasal cavity via their natural breathing. Generally, the mice have recruited immunization every 10 days, totally immunized three times. 10 days after the final immunization, the mice were sacrificed for further experiments. Blood and bronchoalveolar lavage fluid (BALF) were collected.

For further experiments, to prepare the sample, serum was harvested from the blood after centrifuging at 4500rpm, 15 minutes, 4℃. And the BALF was collected from the supernatant.

2.2.10 Anti-OVA ELISA (IgA, IgG)

An Enzyme-linked immunosorbent assay (ELISA) was performed with the different subtypes of antibodies to measure the anti-OVA antibodies level in tissues after immunization. One day before the experiment, a 96-well ELISA plate (Thermo Fisher Scientific; 467320) was coated with 100 μl OVA (200 μg/ml in PBS), incubating at 4℃ overnight. Wash the plate twice after incubation with washing buffer PBS containing 0.01% tween-20, and block the plate with blocking buffer- PBS containing 1%FBS at 37 ℃ for one hour. Wash twice, and the sample (serum or BALF) was added at 10 μl each well after a two-fold serial dilution with PBS. After 2-hour 37℃ incubation, 5 times washing was performed, and HRP-conjugated secondary antibodies were added with a dilution of 1:3000, incubating for another 1 hour, 37℃. Next, O phenylenediamine dihydrochloride (OPD) solution (Thermo Scientific; 34006 and 34062) was added 100 μl per well at room temperature after 5-time washing. When the color developed well, 100 μl 2.5 M H_2SO_4 was added to stop the reaction, and absorbance was measured at 490 mm by spectrophotometer (BMG SPECTRO Star Nano microplate reader).

2.2.11 IgA secretion stimulation

Single cells were isolated from the spleen of either 8-week-old STAP1-*WT* or STAP1-KO mice and seed at the density of $5X10^6$ cells per well in a 24-well plate, culturing RPMI1640 with 20mg/mL LPS, 1ng/mL TGF-β, 5ng/mL IL-5 as IgA stimulation group, while control group cultured with PBS. Cells were collected after 5 days of stimulation[57].

2.2.12 Seahorse XF Cell Mito stress assay

After primary cell isolation and red blood cell lysis, cells were seeded at the density of 10^7 per well and Poly-L-lysine (Sigma, P4832) was coated on each well one hour before cell seeding. Cells were rested in a non-CO2, 37oC incubator for at least 45 minutes before running the seahorse assay. Oligomycin (final concentration 1μM) (Cayman, 11341), FCCP (final concentration 1 μM) (Cayman, 15218) and a mixture of Rotenone (Cayman, 13995) and Antimycin A (Sigma, A8674)(final concentration 0.5 μM each) were injected in sequence. Basel respiratory was recorded for 3 cycles with 30 seconds of the mix, 4 minutes of wait, and 3 minutes of measurement of each cycle. Oxygen consumption rate (OCR) was continuously recorded for 12 cycles, consisting of 30 seconds of the

mix, 4 minutes of wait, and 3 minutes of measurement in each cycle. Protein concentration in each well measured by BCA assay was used to normalize each well after the seahorse assay run.

2.2.13 Seahorse XF Cell Glycolysis stress assay

Primary cells were seeded at the density of 10^7 per well and Poly-L-lysine (Sigma, P4832) was coated on each well one hour before cell seeding. Cells were rested in a non-CO2, 37oC incubator for at least 45 minutes before running the seahorse assay. Glucose (final concentration 10mM) (Sigma, G8270), Oligomycin (final concentration 1μM) (Cayman, 11341), and 2-DG (final concentration 50mM) (Sigma, D8375) were injected in the ports in order. Extracellular acidification rate (ECAR) was continuously recorded for 12 cycles, consisting of 30 seconds of the mix, 4 minutes of wait, and 3 minutes of measurement in each cycle. BCA assay was used to determine the protein concentration for normalization of each well after the seahorse assay run.

2.2.14 LPS and con A stimulation

To investigate the relationship between STAP1 and the proliferation of B cells and T cells, stimulated single cells from the spleen with 1 μg/ml LPS, 5 μg/ml conA, and PBS (control) for 3 hours, respectively. Cells were collected for flow cytometry after 3 hours of stimulation.

2.2.15 Bone marrow-derived dendritic cell (BMDC) differentiation

200 ng/ml FMS-like tyrosine kinase 3 (Flt3-L) ligand (PeproTech; 250-31L) was added in single cells from bone marrow to differentiate into dendritic cells for 9 days. Flow cytometry was used to check the purity of BMDCs staining with surface markers PE-CD11c and APC-MHC class II. Besides, to detect the activation of BMDCs by LPS, 1 μg/ml LPS and PBS (control) was added to the cells after 9-day differentiation incubating at 37^{o}C, at least 15 hours. Cell activated surface markers CD80 and CD86 were stained after incubation. To confirm the intracellular expression of IL-1β and IL-6, Foxp3/Transcription Factor staining buffer was used refer to the information sheet (Thermo; 00-5523).

2.2.16 MitoTracker staining

After the surface marker staining, the staining cells were washed with FACS buffer. Discard the supernatant after centrifuge, and resuspend the cells pellet with the pre-warmed MitoTracker probes, including MitoTracker Green, MitoTracker Red, or MitoSox. Incubate for 15 minutes at 37℃. Once the staining time was over, FACS was added to wash the cells, and cells would be got after centrifuge. Finally, the cells were resuspended with FACS, which were ready to use for flow cytometry.

2.2.17 Statistical analysis

GraphPad Prism 7 was used to analyze the data, and all data were shown as mean ± SEM. Statistical significance was determined with an unpaired Student's t-test. A P-value lower than 0.05 was considered statistically significant and labeled with *, while a lower than 0.01 was label with **.

Chapter 3- STAP1 is essential for maintaining the immune response

3 STAP1 is essential for the immune response regulation

3.1 Introduction

In the last decades, STAP1 is primarily studied as the fourth causative gene of hypercholesterolemia, which make it be ignored that STAP1 is mainly expressed in immune cells, including B cells, T cell, dendritic cell, and macrophage. It is worth noting that, the immune cell-expressing STAP1 might generally function in immune response regulation.

STAP1 is initially identified as the substrate of Tec, which was related to the intracellular signalling mechanism of cytokine receptors, acting a vital role in the immune system by controlling immune functions[35-36]. Also, in Romas cells, *it is* proved that STAP1 activateS c-AMP-response element binding protein activity after B cell receptor (BCR) accumulation[49]. With the epidemic of COVID-19, more and more researchers focuse on studying epidemiology. STAP1 is listed as one of the ten top differentially expressed genes in COVID-19 patients' lungs relying on sequencing analysis, compared with healthy lungs [56]. More and more evidences point out that STAP1 functions on immune system management, which is still unclear to clarify. s

Thus, in this chapter, I designed the nasal immunization assay using STAP1-WT and STAP1-KO mice to explain whether STAP1 controlled the immune response.

3.2 Result

3.2.1 *STAP1* is mainly expressed in B cells

To validate the STAP1 gene deletion on the C57BL/6J mice, primers were designed according to the global knockout mice generation targeting strategy (Figure 3.2.1 A). The forward primer was located on exon 2, while the reverse primer was placed on exon 5. Therefore, the genotyping primers were designed across the exon 5 to identify the STAP1-WT and STAP1-KO mice, which small size band of 236bp represented STAP1-KO mice, 266bp band represented STAP1-WT mice and double bands with 236bp and 266bp represented heterogeneous mice (Figure 3.2.1 B). Splenic single cells were isolated from STAP1-WT or STAP1-KO mice, and a Microbeads B cell negative isolation kit was used to purify B cells for further verification. Total RNA from purified B cells was extracted for RT-qPCR analysis. It was undetectable in B cells from STAP1-KO mice (Figure 3.2.1 C). Besides, the lysis of purified B cells was for immunoblotting analysis. There was no product to show the presence of STAP1 protein expression (Figure 3.2.1 D). Double confirmation with RT-qPCR and immunoblotting analysis demonstrated the successful deletion of STAP1 in the STAP1-KO mice.

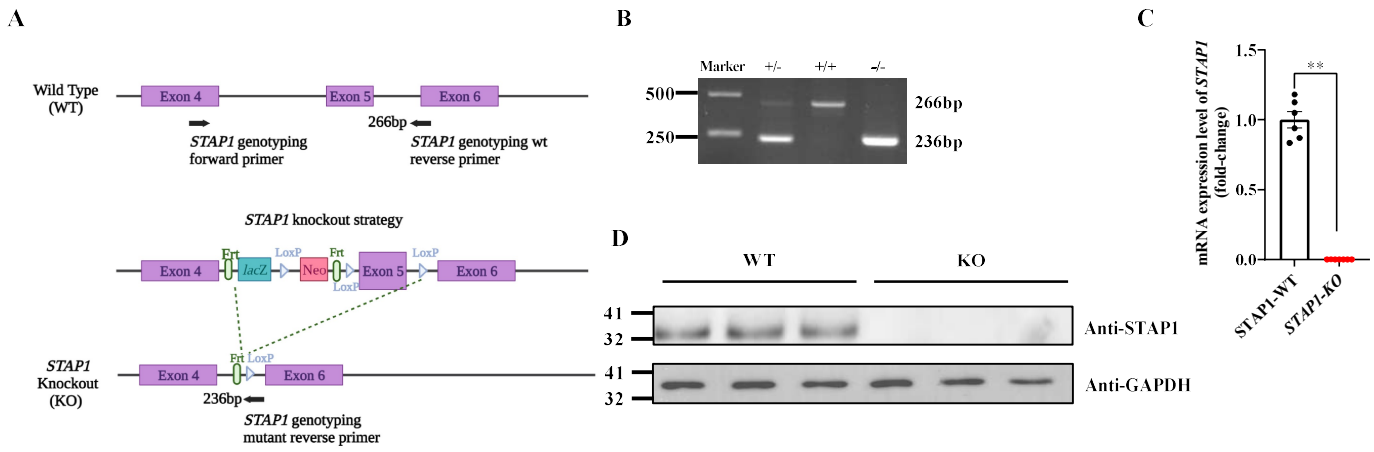

Figure 3.2.1 STAP1 knockout validation. STAP1 knockout (KO) mice were generated using the knockout-first strategy (A). The validity of the KO genotype was confirmed by PCR analyzing the ear tissue (B), real-time RT qPCR analyzing the spleen sample (C), and western blot analyzing the spleen (D). Data are expressed as mean ± SEM, *indicated a significant difference, *$p < 0.05$; **$p < 0.01$; ***$p < 0.001$ (n=3). Each dot represents the measurement of an individual mouse, and the column indicates the average.

Referring to the database, STAP1is mainly expressed in immune tissues, including bone marrow, thymus, spleen, appendix, and lymph node. Therefore, which type of immune cells had the highest expression level of STAP1 was vital for further study. The population of main immune cells in the spleen was checked by flow cytometry after single cell isolation of STAP1-WT mice. Based on the gating strategy (Figure 3.2.2 A) to distinguish B cells, T cells, dendritic cells, and macrophages, the biggest population of B cell was detected in the spleen (Figure 3.2.2 B). Followed by the RT-qPCR analysis to measure the STAP1 mRNA

expression level, the result indicates that, STAP1 was mainly expressed in B cells in the spleen (Figure 3.2.2 D). RT-qPCR was also conducted with the markers of B cell (CD19), T cell (CD3), dendritic cell (CD11c), and macrophage (F4/80) markers to verify the purity of different isolated immune cells (Figure 3.2.2 C). The STAP1 mRNA expression levels among the major types of sphenic B cells, namely naive B cells (IgM^+ IgD^+), active B cells (IgM^-IgD^-) and plasmablasts ($B220^{low}CD138^+$), were similar as determined by RT-qPCR (Figure 3.2.3 A and B).

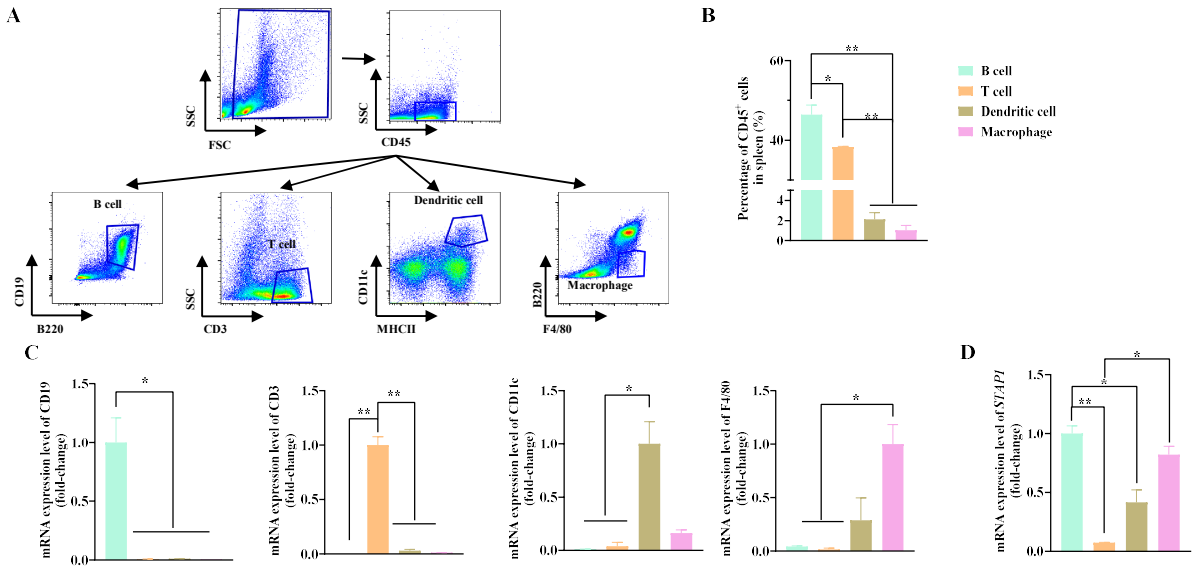

Figure 3.2.2 STAP1 is mainly expressed in marine B cells. Mouse spleens were collected from 8-week-old mice on STC for single cell preparation, followed by flow cytometry for immune cell profiling. (A-B) $CD45^+$ B cells ($B220^+CD19^+$), T cells ($CD3^+$), dendritic cells ($CD11c^+MHC\text{-}II^+$) and macrophages ($B220^-F4/80^+$) in the spleen were gated as indicated (A). Quantification of the frequencies of various immune cell types in the spleen (B). (C-D) Individual immune cell types were purified by microbeads using CD19 as a marker for B cells, CD3 for T cells, CD11c and MHC-II for dendritic cells, and F4/80 for macrophage, and their purities were confirmed using RT-qPCR (C). mRNA expression levels of STAP1 in immune cells were assessed using RT-qPCR (D). Data are expressed as mean ± SEM, *indicated a significant difference, *$p < 0.05$; **$p < 0.01$; ***$p < 0.001$ (n=3). The column indicates the average.

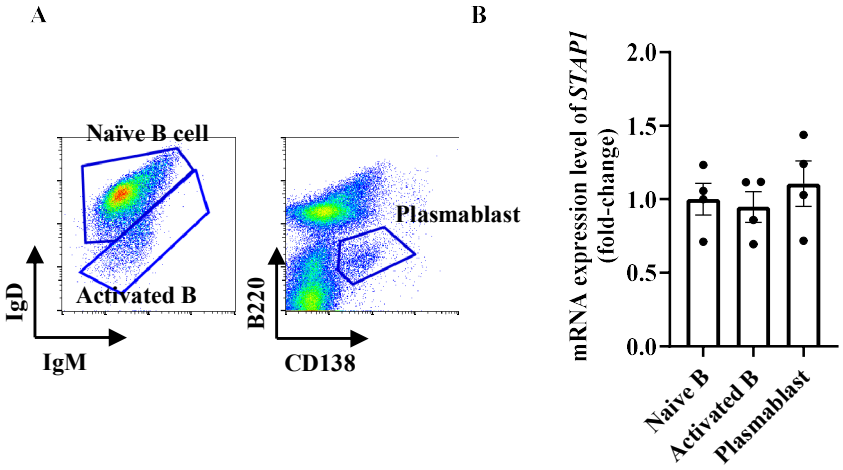

Figure 3.2.3 STAP1 expresses similar level in various subsets of B cell. Splenocytes were initially gated as in Figure3.2.4 (A) for identifying relevant cell populations, which were sorted for obtaining B cell subsets including naïve B cells ($CD45^+B220^+CD19^+IgD^+IgM^+$), activated B cells ($CD45^+B220^+CD19^+IgD^-IgM^-$) and plasmablasts $CD45^+B220^{mid}CD138^+$) (A). Expression levels of STAP1 in these B cell subsets was determined by RT-qPCR (B). Data are expressed as mean ± SEM. *indicated a significant difference, *$p < 0.05$; **$p < 0.01$; ***$p < 0.001$ (n=3). Each dot represents the measurement of an individual mouse, and the column indicates the average.

3.2.2 Lack of STAP1 reduces IgG and IgA secretion after immunization

According to the study from Saxena group, STAP1 is listed as the top gene that significantly increased in COVID-19 patients' lungs, compared with healthy individuals. Besides, STAP1 is mainly expressed in B cells, which largely function in antibody production. I hypothesized that STAP1 acted as an important role in the regulation antibodies secretion. Therefore, I checked the population of the B cell subtype in the blood, spleen, and liver of STAP1-KO mice and its wildtype littermates and conducted the immunization experiment with STAP1 WT and KO mice, using OVA and different adjuvants, to confirm whether STAP1 was required for immune response maintenance.

The population of the antibody-secreting-related B cell subtype, including naïve B cells, activated B cells and plasmablasts were measured by flow cytometry. There was no significant change in the population of these three cells in the blood, spleen, and liver of STAP1-WT and STAP1-KO mice (Figure 3.2.4).

S100A4 was used for mucosal immunization in my experiment, which was because S100A4 had been involved as crucial for mucosal immunization[58], and it is proven that it works to boost the antibodies production as an adjuvant[59]. In addition, cholera toxin was also used as the strong adjuvant in this immunization, and it is

the most well-known immunostimulatory. Cholera toxin is an exotoxin generated by Vibrio cholerae and in charge of inducing cholera diarrhoea, which has been declared to be a gold standard mucosal adjuvant for research use[60-61]. In my immunization experiment, 8-week-old STAP1-WT and KO mice were immunized with OVA or OVA with S100A4 (10 mg) or cholera toxin(CT, 1 mg). Referring to my preliminary experiment, similar results could be got after the first immunization and the second immunization. Hence, to grab the right endpoint to measure the capacity of antibody production, mice were sacrificed 3 days or 10 days after the first immunization or the third immunization. Serum and bronchoalveolar lavage fluid (BALF) was collected for the enzyme-linked immunosorbent assay (ELISA). To harvest the serum from mice, whole blood was collected from the orbit and centrifuged at 4500rpm, for 15 minutes. The supernatant was transferred to another tube as serum. For BALF collection, mice bronchus was cut and 1mL PBS was injected from the small incision using a 1mL syringe. The liquid was withdrawn after at least 1 minute, which was regarded as BALF after centrifuging 1000rpm, and 5 minutes to discard the cells in the bottom.

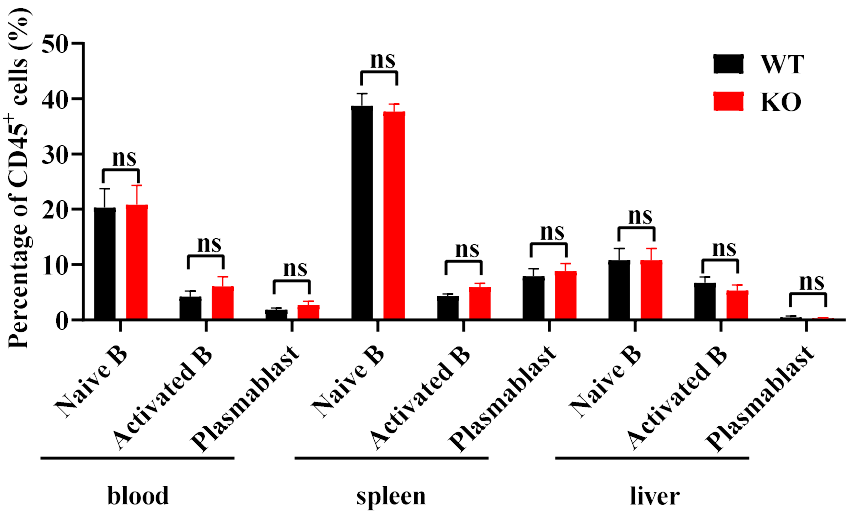

Figure 3.2.4 There is no significant change in the population of the B cell subtype in both STAP1-WT and STAP1-KO mice. Tissues as indicated were collected from 8-week-old STAP1-WT or STAP1-KO mice on STC followed by flow cytometric analysis to determine the frequencies of various B cell subset. Quantification of the frequencies of naïve B cells, activated B cells and plasmablasts is shown based on the gating strategy in Figure 3.2.5 A. Data are expressed as mean ± SEM (n = 3). Each dot represents the measurement of an individual mouse, and the column indicates the average.

For the immunization assay, mice were immunized with OVA, the major protein component in chicken egg white, intranasally. OVA was used as the experimental vaccine in the whole study. Firstly, I sacrificed the immunized mice 10 days after the first immunization with S100A4 or CT (Figure 3.2.5 A), and serum and BALF were collected for anti-OVA titer ELISA. The ELISA data showed that, after immunization, in the STAP1-WT group, the BALF IgA, serum IgG and IgG2c

increased after being immunized with S100A4 or CT, compared with immunized only with OVA (Figure 3.2.5 B-D). That was to say, the immunization assay successfully boosted the immune response after adjuvant activation. And when it came back to comparing the STAP1-WT and STAP1-KO groups, the column revealed that no matter in the S100A4 group or CT group, mice lacking STAP1 secreted fewer antibodies, including BALF IgA (Figure 3.2.5 B), serum IgG (Figure 3.2.5 C),and IgG2c (Figure 3.2.5 D).

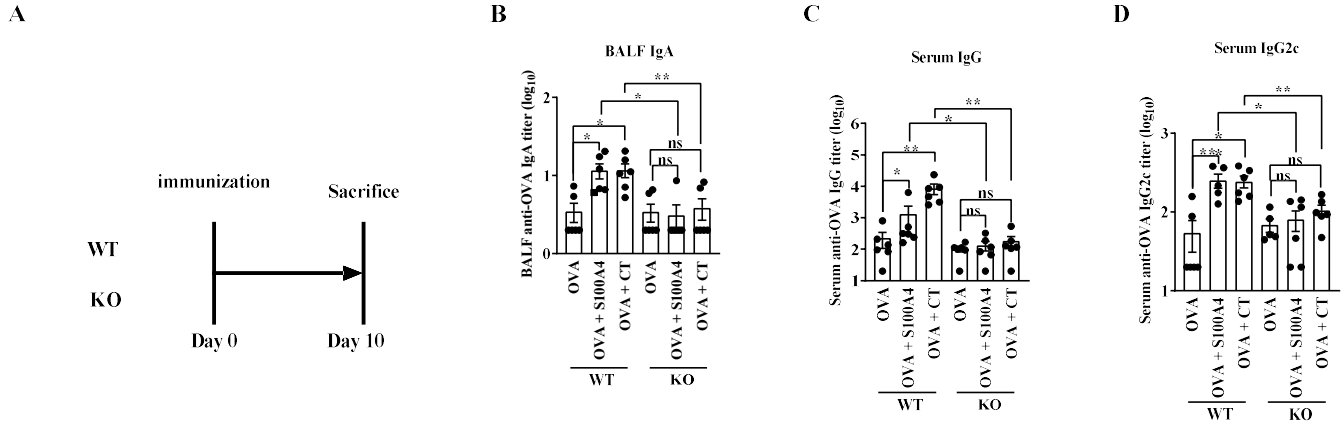

Figure 3.2.5 Lack of STAP1 reduces antigen-specific antibody production after mucosal immunization. 8-week-old STAP1-WT or STAP1-KO mice were intranasally immunized with ovalbumin (OVA) in the presence or absence of S100A4 or cholera toxin (CT) as an adjuvant. Mice were scarified 10 days after the immunization (A), and the bronchoalveolar fluid (BALF) and serum were collected for determining the anti-OVA IgA in BALF (B), total IgG (C) and IgG2c (D) in serum using ELISA. Data are expressed as mean ± SEM (n = 6). Each dot represents the measurement of an individual mouse, and the column indicates the average.

To further confirm whether STAP1 was essential for immune response, mice were sacrificed 3 days after the third immunization assay to check whether STAP1 expression was necessary for germinal centre B cells generating antibodies (Figure 3.2.6 A). A lower level of BALF IgA (Figure 3.2.6 B), serum IgG (Figure 3.2.6 C),and IgG2c (Figure 3.2.6 D) were found in the STAP1-KO group after S100A4 or CT immunization, which indicated that deficiency of STAP1 impaired the function of germinal centre B cells on antibodies production.

To better investigate the relationship between STAP1 and immune response, mice were sacrificed 10 days after the third immunization. Interestingly, the lesser antibody level could be also detected in BALF IgA (Figure 3.2.7 B), serum IgG (Figure 3.2.7 C),and IgG2c (Figure 3.2.7 D) of the STAP1-KO group after S100A4 or CT immunization, compared with the STAP1-WT group.

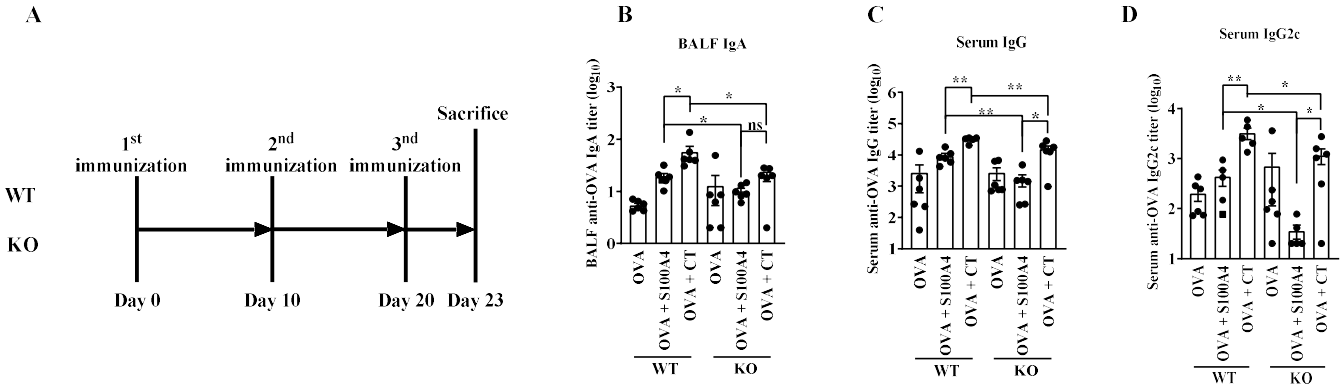

Figure 3.2.6 STAP1 deficiency reduces antigen-specific antibody production after mucosal immunization. 8-week-old STAP1-WT or STAP1-KO mice were intranasally immunized with ovalbumin (OVA) in the presence or absence of S100A4 or cholera toxin (CT) as an adjuvant. Mice were intranasally immunized as described above for three times and tissues were harvested 3 days after the last immunization (A), and BALF and serum were collected for determining the anti-OVA IgA in BALF (B), total IgG (C) and IgG2c (D) in serum using ELISA. Data are expressed as mean ± SEM (n = 6). Each dot represents the measurement of an individual mouse, and the column indicates the average.

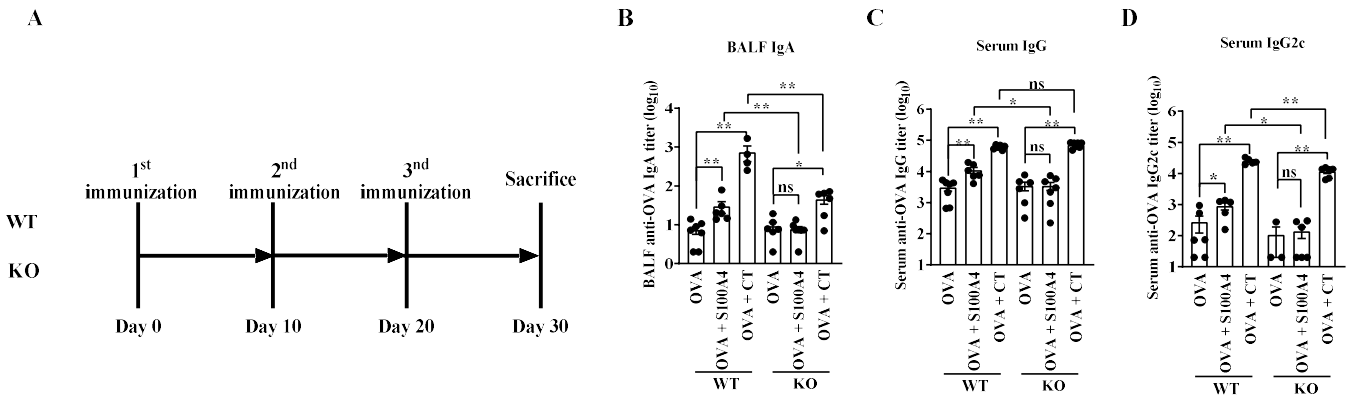

Figure 3.2.7 Absence of STAP1 reduces antigen-specific antibody production after mucosal immunization. 8-week-old STAP1-WT or STAP1-KO mice were intranasally immunized with ovalbumin (OVA) in the presence or absence of S100A4 or cholera toxin (CT) as an adjuvant. Mice were intranasally immunized as described above for three times and tissues were harvested 10 days after the last immunization (A), and BALF and serum were collected for determining the anti-OVA IgA in BALF (B), total IgG (C) and IgG2c (D) in serum using ELISA. Data are expressed as mean ± SEM (n = 6). Each dot represents the measurement of an individual mouse, and the column indicates the average.

3.2.3 Deletion of STAP1 decreases the population of the bone marrow-derived dendritic cells but does not affect its activation after stimulation

Based on the pathway after antigens get into our bodies, they first meet with the antigen-presenting cells, for example, the dendritic cell (DC). Secondly, they will be phagocytosed into small fragments and presented to the Naïve T cell by DC. Meanwhile, antigen fragments act as stimulators to trigger naïve T cell differentiation. The Naïve T cell will differentiate into two different T helper (Th) cells based on the different antigens, Th1 and Th2 cells, which can activate B cell differentiation and plasma B cell to secrete antibodies ultimately. To further know how STAP1 maintain the immune response, I stimulated the splenic single cells and single cells from bone marrow of either STAP1-WT or STAP1-KO mice with different stimulators to measure whether there was any change in the activation of dendritic cell, T cell, and B cell.

For dendritic cell activation, single cells were harvested by blushing the bone marrow and differentiated by adding 200 ng/ml FMS-like tyrosine kinase 3 ligand (Flt3-L). The bone marrow-derived dendritic cell (BMDC) could be collected after 9 days of differentiation, followed by flow cytometry to check the population of differentiated BMDCs (Figure 3.2.8 A). In the STAP1-WT group, the population

of BMDC raised from 34.3% to 95% after 9-day differentiation, which indicated the single cell from bone marrow differentiated effectively into the dendritic cell. Compared with the STAP1-WT group, single cells from the bone marrow of STAP1-KO mice had a lower efficiency of differentiating into the dendritic cell (Figure 3.2.8 B). Next, 1μg/mL LPS was added in the BMDC of STAP1-WT or STAP1-KO group to measure the activation capability, and PBS was added as the control. Flow cytometry was applied for BMDCs activation assessment (Figure 3.2.9 A). In both the STAP1-WT and STAP1-KO group, the elevated number of CD80 and CD86 could be found after stimulation, which suggested the effective stimulation assay. Remarkably, there was no change in surface markers CD80 and CD86 after stimulation between the two groups (Figure 3.2.9 B).

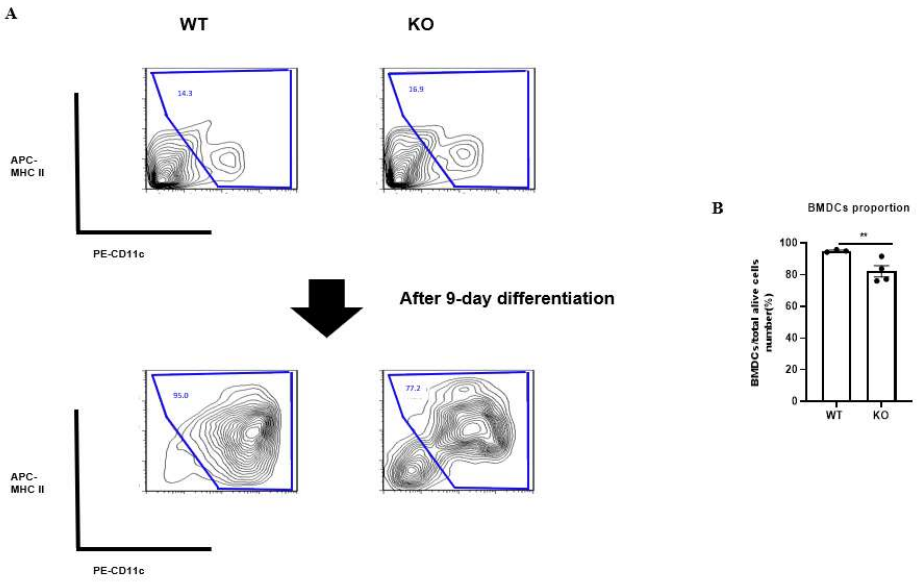

Figure 3.2.8 Deletion of STAP1 decreases the population of the bone marrow-derived dendritic cell. 8-week-old STAP1 KO and WT mice were sacrificed and bone marrow were collected for single cells isolation by blushing with PBS. 200 ng/ml FMS-like tyrosine kinase 3 ligand (Flt3-L) was added to differentiate. 9-days after differentiation, cells were collected for flow cytometry with surface marker MHC- II and CD11c to determine the bone marrow-derived dendritic cells (BMDCs) (A). The population of the bone marrow-derived dendritic cell Quantification of the frequencies of BMDCs in of STAP1-WT or STAP1-KO mice are shown (B). Data are expressed as mean ± SEM (n = 3-4). Each dot represents the measurement of an individual mouse and the column indicates the average.

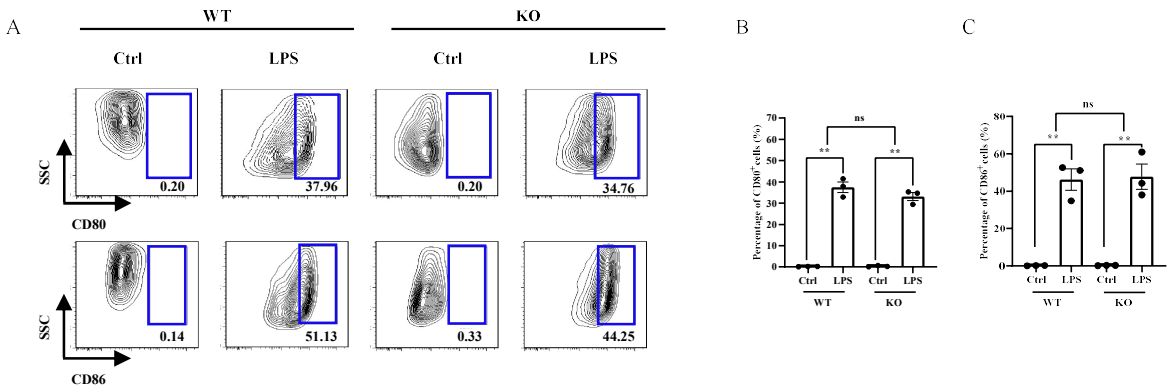

Figure 3.2.9 STAP1 deficiency does not impact on proliferation and activation of dendritic cells. Single cells isolated from the bone marrow of STAP1-WT or STAP1-KO mice were cultured in the presence of Flt3-L for dendritic cell differentiation. After 9 days of culture, bone marrow-derived dendritic cells (BMDC) were collected and stimulated with 1 mg/ml lipopolysaccharide (LPS). Cells were analyzed for activation using flow cytometry by first gating on CD11c+MHC class II+ population (not shown), followed by assessing the activation markers CD80 and CD86 (A). (B) Quantification of the frequencies of CD80+ (B) or CD86+ (C) BMDCs is shown. Quantification of the frequencies of CD3+ T cells is shown. Data are expressed as mean ± SEM (n = 3). Each dot represents the measurement of an individual mouse and the column indicates the average.

3.2.4 Obliteration of STAP1 does not affect the population of T cells after stimulation

After encountering the antigen-presenting cell, the antigen should be phagocytosed into small fragments and presented to the Naïve T cell by DC. Hence, I planned to stimulate the single splenic cells from STAP1-WT or STAP1-KO mice with 5μg/mL conA or PBS for 2 hours to verify the link between STAP1 and T cell activation. Followed by collecting cells for flow cytometry (Figure 3.2.10 A). Surprisingly, there was no difference in the T cell population between the two groups after stimulation (Figure 3.2.10 B).

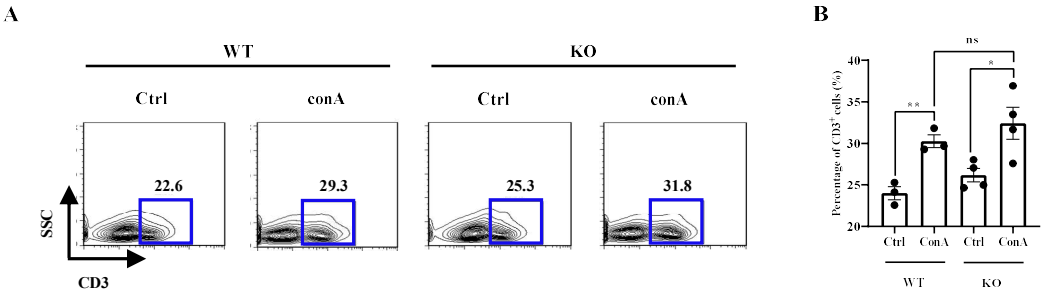

Figure 3.2.10 STAP1 deficiency does not impact on proliferation and activation of T cells. Splenocytes from STAP1 WT or KO mice were stimulated with conA (5μg/ml) for 2 hours, followed by T cell frequency analysis using flow cytometry by gating on CD3+ cells (D). Quantification of the frequencies of CD3+ T cells is shown. Data are expressed as mean ± SEM (n = 4). Each dot represents the measurement of an individual mouse and the column indicates the average.

3.2.5 Absence of STAP1 moderates B cells IgA-class switching and IgA secretion after stimulation ex vivo.

Excluding the impact of STAP1 impairing the activation of dendritic cells or T cells, I further focused on the activation of B cells, including the antibodies production and immunoglobulin class switching. Based on the in vivo assay result, STAP1 mostly altered the mucosal antibody secretion, which was primarily made up of IgA, I intended to stimulate the single splenic cells with 20mg/mL LPS, 1ng/mL human TGF-β and 100U/mL IL-5 for 6 days to validate the B cell activation. Flow cytometry using surface markers B220, CD138, and intracellular marker IgA were performed to confirm the immunoglobulin class switching. Anti-IgA ELISA was conducted to measure antibody production. Higher IgA-class switching B cells ($B220^{high}IgA^{+}$ or $B220^{mid}IgA^{+}$) and plasma B cells observed in the IgA stimulation group of WT mice implied that the IgA was stimulated effectively. Consistent with the in vivo experimental results, a lesser concentration of IgA secretion was detected from isolated single splenic cells from STAP1-KO after stimulation (Figure 3.2.11 E). Similarly, single splenic cells from STAP1-KO mice had a smaller amount of IgA-class switching B cells ($B200^{high}IgA^{+}$ or $B220^{mid}IgA^{+}$) and plasmablasts compared with the stimulation group of STAP1-

WT mice (Figure 3.2.11 B-D). To further validate this finding, we measured IgA antibody production in the cell culture supernatant by ELISA. In agreement with those observations, lower levels of IgA antibodies were detected in the culture supernatants of stimulated splenic B cells derived from STAP1-KO mice than B cells from their WT littermates (Figure 3.2.11 E).

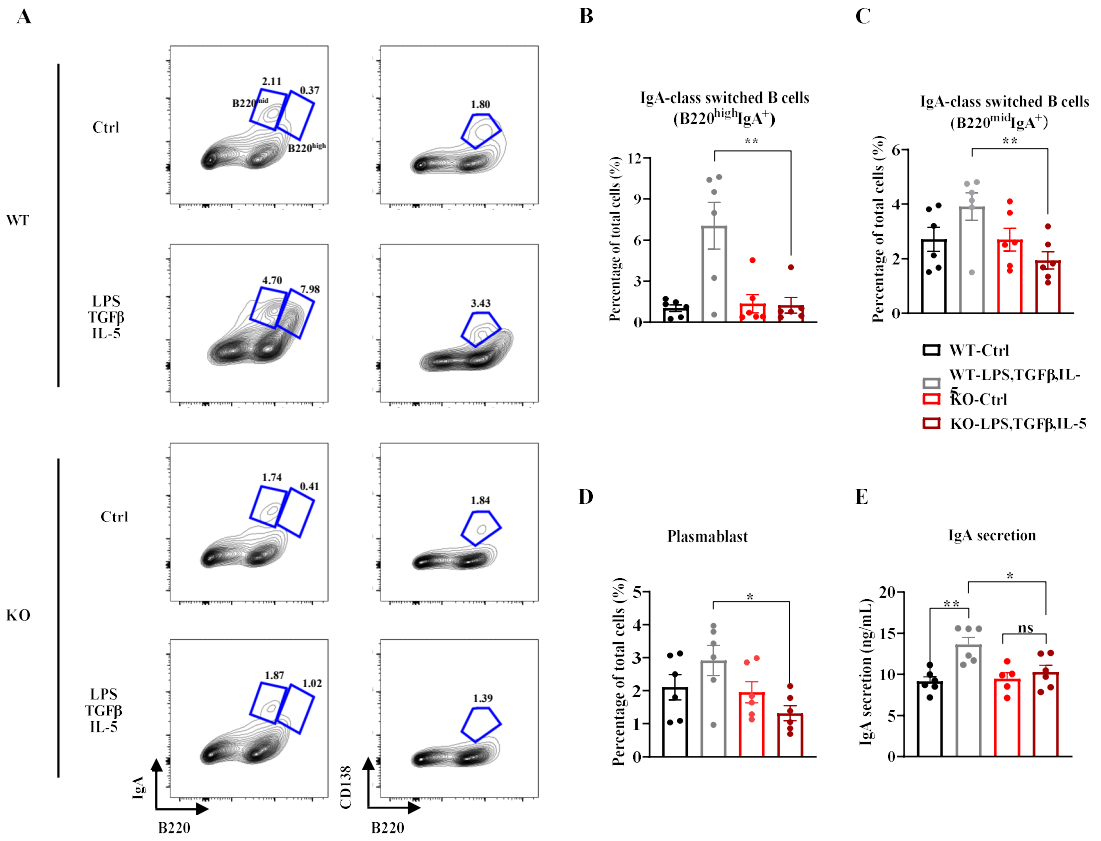

Figure 3.2.11 STAP1 deficiency suppresses IgA-class switching and IgA secretion by B cells after stimulation ex vivo. Spleen single cell suspensions were prepared from either 8-week-old STAP1-WT or STAP1-KO mice, followed by culture in medium containing 20 mg/mL lipopolysaccharide (LPS), 1 ng/mL TGF-β, 5 ng/mL IL-5 for promoting class switch to IgA, while the control (Ctrl) cells were cultured with medium supplemented with PBS. Cells were collected after 5 days of culture. (A-D) Cells were analyzed by flow cytometry for identifying various B cell subsets as indicated (A). The population frequencies of various B cell subsets with IgA expression (B and C), plasmablasts (D). (E) Cell culture supernatants were examined for the concentration of secreted IgA using ELISA. Data are expressed as mean ± SEM (n = 4-6). Each dot represents the measurement of an individual mouse and the column indicates the average.

3.2.6 Knockdown STAP1 in hybridoma B cells reduces the antibody secretion.

STAP1 KO mice were demonstrated to induce fewer antibodies after stimulation, compared with the WT mice in vivo or ex vivo. To study more about this phenotype, I also investigated whether there would get the same result from other models. Hybridoma B cell with the antibody-generating ability of B cell and long life and reproductivity of the myeloma was used for further study [62-63]. For the hybridoma B cell I used in this study, IgG1 is mainly secreting antibody subclass. To knock down the STAP1 expression in the hybridoma B cell, siRNA and lipofect2000 were used. Two different siRNA-STAP1were applied for this assay at a concentration of 10μM. The mRNA expression level and STAP1 protein expression level of STAP1 was measured to confirm the efficiency of siRNA knockdown. Declined mRNA expression level (Figure 3.2.12 A) and protein expression level (Figure 3.2.12 B and C) of STAP1 in siRNA-STAP1 groups implies the effective knockdown STAP1 model using hybridoma B cells. Again, the diminishing titer of IgG1 was measured in the siRNA-STAP1 knockdown group by ELISA, compared with its controls (Figure 3.2.12 D).

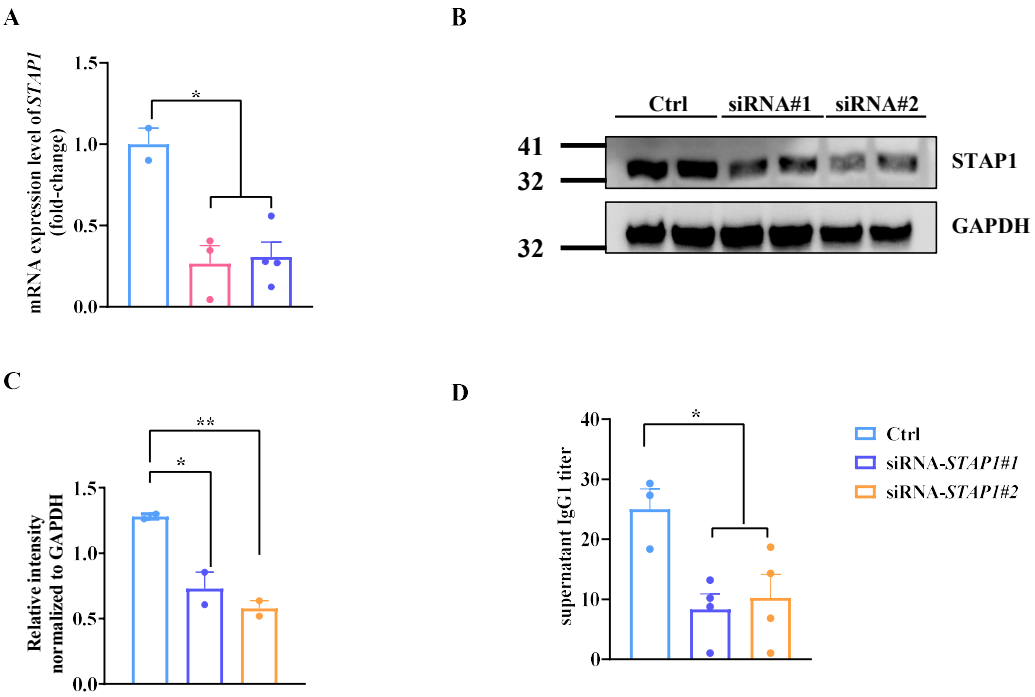

Figure 3.2.12 Knockdown STAP1 diminishes the titer of IgG1. Hybridoma B cells were transfected with 10μM siRNA-Ctrl and 10μM siRNA-STAP1. Cells were collected 24 hours after transfection for RNA extraction, and RT-qPCR was conducted to determine the mRNA expression level of (A) STAP1 and protein expression level of STAP1 (B and C). ELISA was performed 48 hours after transfection. The titer of IgG1 in the culture medium was measured (D). Data are expressed as mean ± SEM (n = 4). Each dot represents the measurement of an individual mouse, and the column indicates the average.

4.3 Summary

STAP1 is supposed to function in immune system regulation. Especially with the development of the COVID-19 epidemic, STAP1 is listed in the first place of related genes[56], which makes us pay more attention to how STAP1 mediates the immune response. That may be a clue to better understanding the mechanism of COVID.

As COVID mainly affected lung damage, I chose the nasal immunization method to investigate the link between STAP1 and immune response. 10-days after the first immunization or 3-days after the third immunization, the lower level of antibodies, including serum IgG, BALF IgG, and IgA were measured in STAP1-KO mice under both two adjuvants, compared with its corresponding wild type controls. Interestingly, 10-days after the third immunization, only serum IgG2c and BALF IgA were discovered fewer production in STAP1-KO mice under the standard adjuvant cholera toxin, and it showed no significant change in serum IgG. Under the novel adjuvant S100A4, the absence of STAP1 displayed a weak reaction to the immune response in both serum and BALF antibodies. To further confirm the phenotype of STAP1 deficiency that harmed the ability of antibody secretion and which part of the immune response activation pathway dysfunction, ex vivo assay

using splenic single cells or single cells from the bone marrow of STAP1-WT and STAP1-KO mice. After stimulation, the differentiation ability of bone marrow-derived dendritic cells dropped in STAP1-KO mice, but it did not alter the activation capability of the bone marrow-derived dendritic cell. Besides, the absence of STAP1 did not have an effect on T cell activation after stimulation. To double-check the ability of antibody generation, after culture with the stimulators, splenic single cells from STAP1-KO mice produced less IgA in the culture medium and the ability of moderating the B cell class-switching weakened. Based on these findings, I also examined the capacity of antibody production using hybridoma B cells transfected with siRNA-STAP1. The data showed that knockdown of the expression of STAP1 diminished the secretion of IgG1 antibody, which was consistent with the result from in vivo or ex vivo.

In this chapter, I demonstrated that deficiency of STAP1 showed a weaker reaction to immune response no matter under a strong adjuvant cholera toxin or a weak adjuvant S100A4. A similar result could be found ex vivo and in vitro using knock down the expression of STAP1. And the ex vivo assays also suggested that the reason why the deletion of STAP1 damaged the ability of antibody production, was due to the abnormal B cell activity instead of the activation of dendritic cells or T

cells. Interestingly, the ability of antibody production displayed differently at various time points after immunization under distinct adjuvants with distinct functional pathways. That might be some hints to clarify how STAP1 functions in controlling the immune response.

Chapter 4- Deletion of STAP1 impairs immune response via mitochondrial dysfunction

4 Deletion of STAP1 impairs immune response via mitochondrial dysfunction

4.1 Introduction

To further learn more about the mechanism of how STAP1 impairs the function of antibody production, cell-based influenced by STAP1 should be noted. Based on the previous chapter suggests that STAP1 may regulate glucose homeostasis, which implies STAP1 is necessary for normalizing the generation of ATP as well [64]. Besides, it is demonstrated that to support their antibodies-producing function, activated germinal centre B cells need fatty acid oxidation and glycolysis to produce energy [16-17]. It is a rising topic in immunometabolism, which is described by combining the words of immunology and metabolism. That is to say, abnormal cell-based metabolic progress in immune cells may cause metabolic diseases or immune diseases [18].

In this chapter, STAP1-KO mice and their controls were used for cell-based metabolic change investigation, mainly included the mitochondrial number and function. Seahorse Extracellular Flux Analyzer was the main tool to measure mitochondrial respiration to determine the main function of mitochondrial- ATP production. Additionally, the glycolysis ability of B cells was also measured using

the Seahorse Extracellular Flux Analyzer. In addition, MitoTracker staining was applied to further confirm the function of mitochondria. Moreover, the complex of mitochondria was quantified by western blot. Co-immunoprecipitate was also applied to check the interaction protein of STAP1 to clarify the STAP1 affected the immune response via impacting the mitochondrial function.

4.2 Result

4.2.1 Knockdown STAP1 impairs mitochondrial respiration and glycolysis

In chapter 3, hybridoma B cells transfected with siRNA-STAP1 were applied to confirm that fewer antibodies were generated after knockdown STAP1 expression. To further verify the hypothesis of the absence of STAP1 harmed the cell-based mitochondrial function to induce the weaker immune response, hybridoma B cells transfected with siRNA-STAP1 were applied for the Seahorse Extracellular Flux Analyzer with different chemicals to determine the capability of ATP production from mitochondrial respiration and glycolysis.

For the mitochondrial stress test to measure mitochondrial respiration after basal respiration measurement, oligomycin was added to inhibit ATP synthase (complex V), damaging the electron flow through the electron transport chain. The area decreasing after oligomycin was regarded as ATP-link respiration. Followed by the injection of FCCP, an uncoupling agent to ruin the proton gradient and interrupt the mitochondrial membrane potential, which allowed electron flow through the electron transport chain to oxygen utilization via complex IV achieved maximum respiration. The final injection of a mixture of rotenone and antimycin A, the complex I and complex III respectively. This mixture interrupted mitochondrial

respiration and permitted the calculation of nonmitochondrial respiration triggered by activities outside the mitochondria.

For glycolysis stress test to measure glycolytic function. Glucose was the first injection for utilization and catabolization by the glycolytic pathway to turn into pyruvate, producing ATP, NADH, water, and proton in the end. In the second step, oligomycin was added as an inhibitor to shift the energy generation to glycolysis, which implied the following raising in extracellular acidification rate (ECAR) was the cellular maximum glycolytic ability. The final step was the injection of 2-DG, a glucose analogy, hindered glycolysis through a competitive tie to glucose hexokinase, the first enzyme in the glycolysis pathway. The subsequent decline in ECAR validated that the ECAR was created in the experiment because of glycolysis. The distinction between glycolytic capacity and glycolysis rate was described as glycolytic reserve.

After 48 hours of siRNA-STAP1 transfection, hybridoma B cells transfected with siRNA-STAP1 displayed a sustained reduction in oxygen consumption rate (OCR) after oligomycin and FCCP injection, compared with their controls (Figure 4.2.1 A). Besides, there was no significant change in the basal respiration measurement between the three groups (Figure 4.2.1 A). Consistently, after analysis, lower levels

of maximal respiration (Figure 4.2.1 B) and spare respiration capacity(Figure 4.2.1 C) were shown in the hybridoma B cells transfected with the siRNA-STAP1 group. In the glycolysis stress test, the hybridoma B cell transfected with siRNA-STAP1 showed a reduction in ECAR (Figure 4.2.2 A), glycolysis, and glycolysis capability (Figure 4.2.2 B, C) after glucose and oligomycin injection.

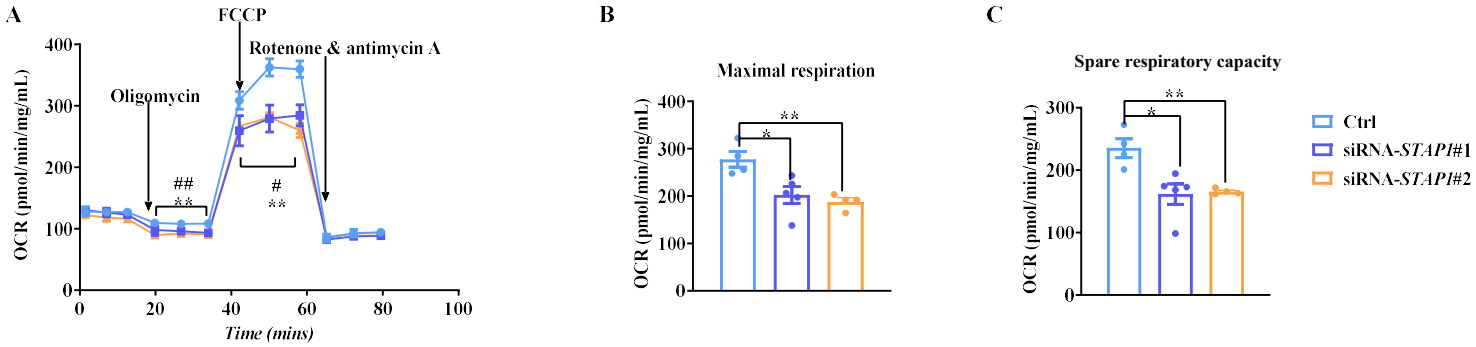

Figure 4.2.1 knockdown of STAP1 reduces mitochondrial respiration. Hybridoma B cells were transfected with 10nM siRNA-STAP1, 10nM siRNA-Ctrl. The Aligent Seahorse XF Cell Mito Stress test was performed to measure the oxygen consumption rate (OCR) (A) in hybridoma B cells after 48 hours of transfection with siRNAs. Extracellular flux analysis of mitochondrial OCR was quantified (B and C). Data are expressed as mean ± SEM. # indicates a significant difference between negative control and siRNA-STAP1#1, # $p < 0.05$; ## $p < 0.01$ (n =5). * indicates a significant difference between negative control and siRNA-STAP1#2, * $p < 0.05$; ** $p < 0.01$;*** $p < 0.001$ (n = 5). Each dot represents the measurement of an individual mouse and the column indicates the average.

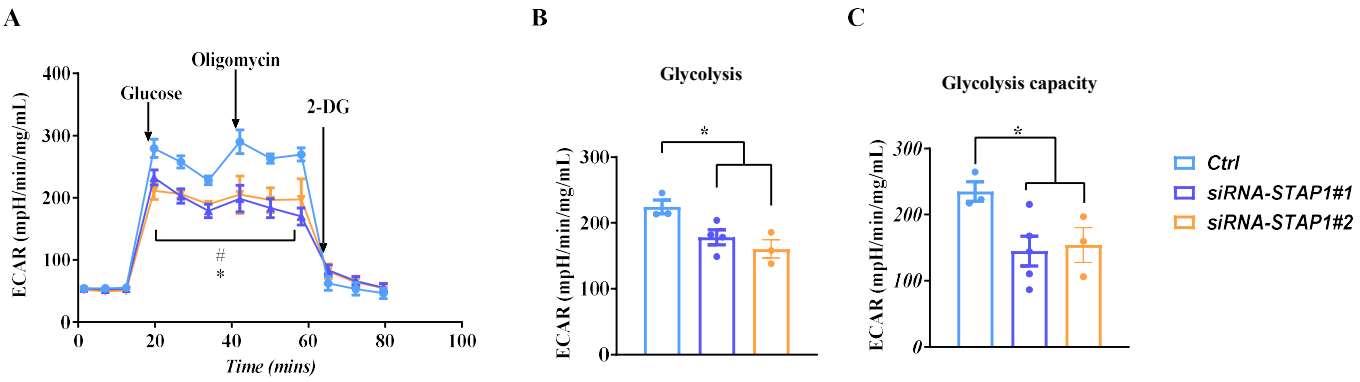

Figure 4.2.2 knockdown of STAP1 diminishes the ability of glycolysis. Hybridoma B cells were transfected with 10nM siRNA-STAP1, 10nM siRNA-Ctrl. Seahorse analysis of the Extracellular acidification rate (ECAR) (A) in hybridoma B cells after 48 hours of transfection with siRNAs. Extracellular flux analysis of ECAR was quantified (B and C). Data are expressed as mean ± SEM. # indicates a significant difference between negative control and siRNA-STAP1#1, # $p < 0.05$; ## $p < 0.01$ (n =5). * indicates a significant difference between negative control and siRNA-STAP1#2, * $p < 0.05$; ** $p < 0.01$;*** $p < 0.001$ (n = 5). Each dot represents the measurement of an individual mouse and the column indicates the average.

4.2.2 Deletion of STAP1 declines mitochondrial respiration and glycolysis

Except for the studies on the knockdown STAP1 cell model, I examined the mitochondrial function using the Seahorse Extracellular Flux Analyzer with primary splenic B cells from STAP1-*KO* mice. Interestingly, lower basal mitochondrial respiration OCR was found in STAP1 deficiency B cells, compared with its controls. Similar to the knockdown model, the lack of STAP1 presented a sustained reduction in OCR after oligomycin and FCCP injection, compared with their controls(Figure 4.2.3 A). Again, drop levels of basal respiration (Figure 4.2.3 B), maximal respiration (Figure 4.2.3 C), and ATP production (Figure 4.2.3 D) were shown in the primary splenic B cell from STAP1-KO mice. In the glycolysis stress test, the primary splenic B cell from STAP1-KO mice revealed a lessening in ECAR (Figure 4.2.4 A), glycolysis (Figure 4.2.4 B), and glycolysis capability (Figure 4.2.4 C) after glucose and oligomycin injection. It was worth to noted that, the primary splenic B cell from STAP1-KO mice had poorer basal glycolysis, compared with their controls.

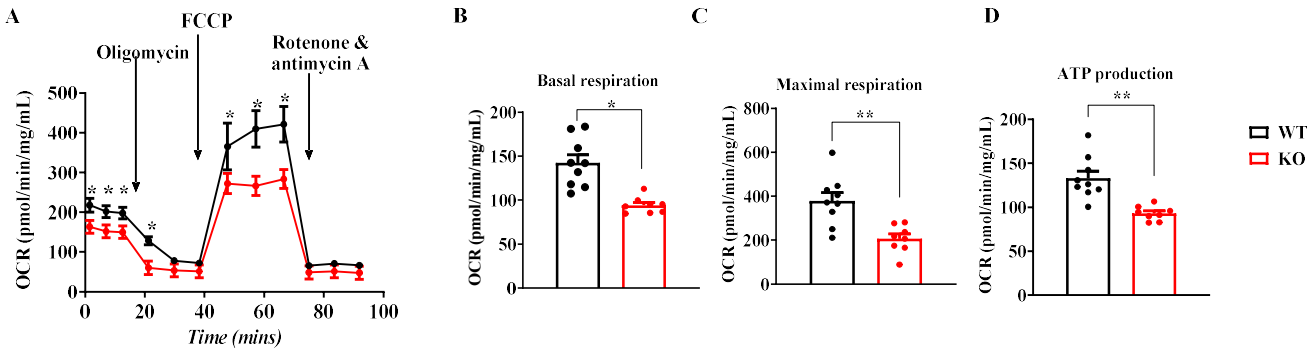

Figure 4.2.3 Loss of STAP1 leads to mitochondrial dysfunction and damage. CD19+ B cells were sorted from splenic cells of either STAP1-WT or STAP1-KO mice using anti-CD19 MicroBeads. The oxygen consumption rates (OCR) were measured using the Aligent Seahorse XF Cell Mito Stress test (A), and the basal respiration (B), maximal respiration (C) and ATP production (D) of mitochondrial OCR were assessed. Data are expressed as mean ± SEM (n = 9-10). * $p < 0.05$; ** $p < 0.01$;*** $p < 0.001$. Each dot represents the measurement of an individual mouse and the column indicates the average.

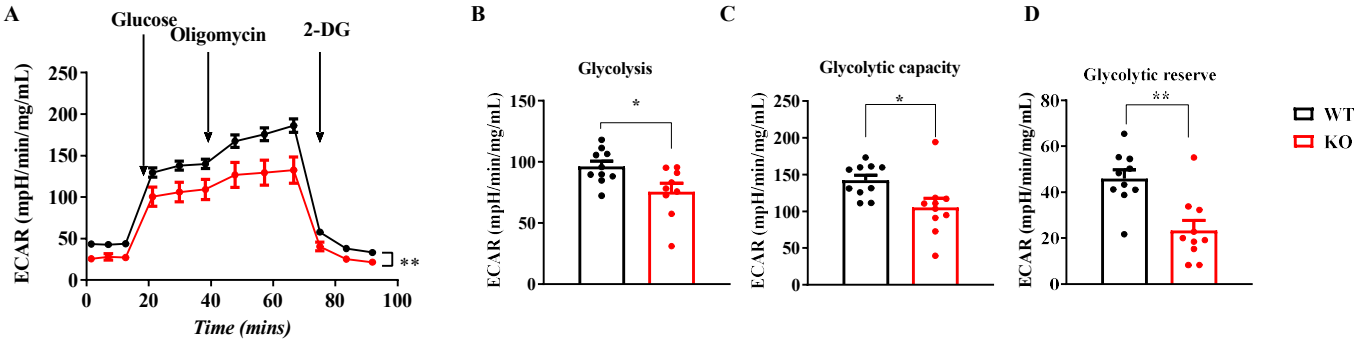

Figure 4.2.4 Loss of STAP1 leads to mitochondrial glycolysis dysfunction. $CD19^+$ B cells were sorted from splenic cells of either STAP1-WT or STAP1-KO mice using anti-CD19 MicroBeads. The extracellular acidification rates (ECAR) were measured using the Seahorse analysis (A), and glycolysis (B), glycolytic capacity (C) and glycolytic reserve (D) were quantified. Data are expressed as mean ± SEM (n = 9-10). * $p < 0.05$; ** $p < 0.01$;*** $p < 0.001$. Each dot represents the measurement of an individual mouse and the column indicates the average.

4.2.3 Knockdown STAP1 drops the gene expression of mitochondrial complexes but does not affect the mitochondrial number

As I found the dysfunctional mitochondria in hybridoma B cell transfected with siRNA-STAP1, to explore whether this abnormal phenotype was related to the number of mitochondria or the biogenesis of mitochondria, I checked the amount of mitochondrial DNA by RT-qPCR first. There was no significant change in the number of mitochondrial DNA between the three groups (Figure 4.2.5 A). Next, I also checked the biogenesis of mitochondria, including mitochondrial transcription factor A (TFAM), NADH-ubiquinone oxidoreductase chain five protein (mtND5) (complex I), cytochrome b (CYTB) complex III), and cytochrome oxidase III (COXIII) （complex IV). Except for TFAM, decreasing mRNA expression levels of mtND5 (Figure 4.2.5 C), CYTB (Figure 4.2.5 D), and COXIII (Figure 4.2.5 E) were discovered in hybridoma B cells transfected with siRNA-STAP1, compared with their controls. There was no significant change in the mRNA expression levels of TFAM between the three groups (Figure 4.2.5 B).

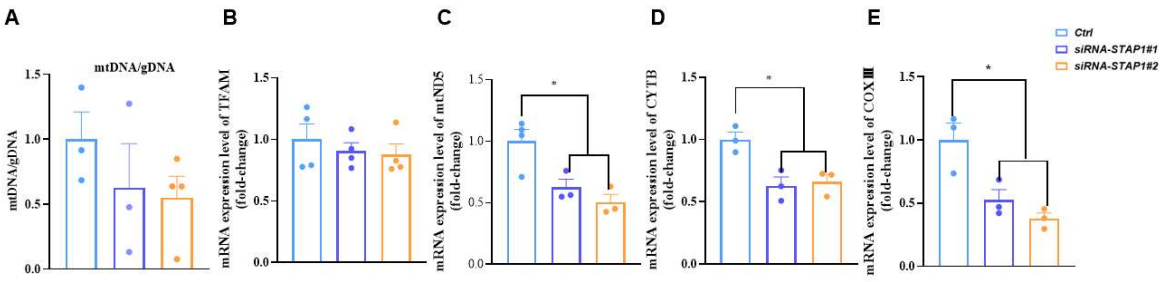

Figure 4.2.5 knockdown STAP1 decreases the mRNA expression of mitochondrial biogenesis. Hybridoma B cells were transfected with 10nM siRNA-STAP1, 10nM siRNA-Ctrl, or its negative control. Cells were collected 24 hours after transfection for RNA extraction, and RT-qPCR was conducted to determine the mRNA expression level of mitochondrial DNA (mtDNA) normalized with genomic DNA (gDNA) (A) and determined the mRNA expression level of mitochondrial biogenesis genes, Mitochondrial transcription factor A (TFAM) (B), NADH-ubiquinone oxidoreductase chain five protein (mtND5) (complex I) (C), cytochrome b (CYTB) (complex III) (D), and cytochrome oxidase III (COXIII) （complex IV) (E). Data are expressed as mean ± SEM (n = 9-10). * $p < 0.05$; ** $p < 0.01$;*** $p < 0.001$. Each dot represents the measurement of an individual mouse and the column indicates the average.

4.2.4 Obliteration of STAP1 diminishes the gene expression of mitochondrial complexes but does not affect the mitochondrial number

MitoTracker Green is a mitochondrial-specific probe that attaches covalently to mitochondrial proteins by responding with cysteine residues and gathers within the mitochondrial matrix [65]. This reaction depends on mitochondrial membrane potential and is used to characterize mitochondrial mass [66].

MitoTracker Red is a probe taken up by polarized mitochondria that are negatively charged [67]. Hence, it is regarded to rely on mitochondrial membrane potential [68]. This probe can be also used to measure the gain or loss of mitochondrial functionality, while the loss is linked with the metabolic move from OXPHOS to glycolysis [69].

Staining with the mixture of these two probes, the mitochondrial function can be determined according to the mitochondrial mass and membrane potential. After staining with two trackers, primary splenic B cells from STAP1-KO mice presented loss of mitochondria, compared with its corresponding wildtype controls (Figure 4.2.6 D), and there was no significant change in the mitochondrial mass between the two groups (Figure 4.2.6 B). Moreover, more dysfunctional

mitochondria were detected in primary splenic B cells from STAP1-KO mice (Figure 4.2.7 B).

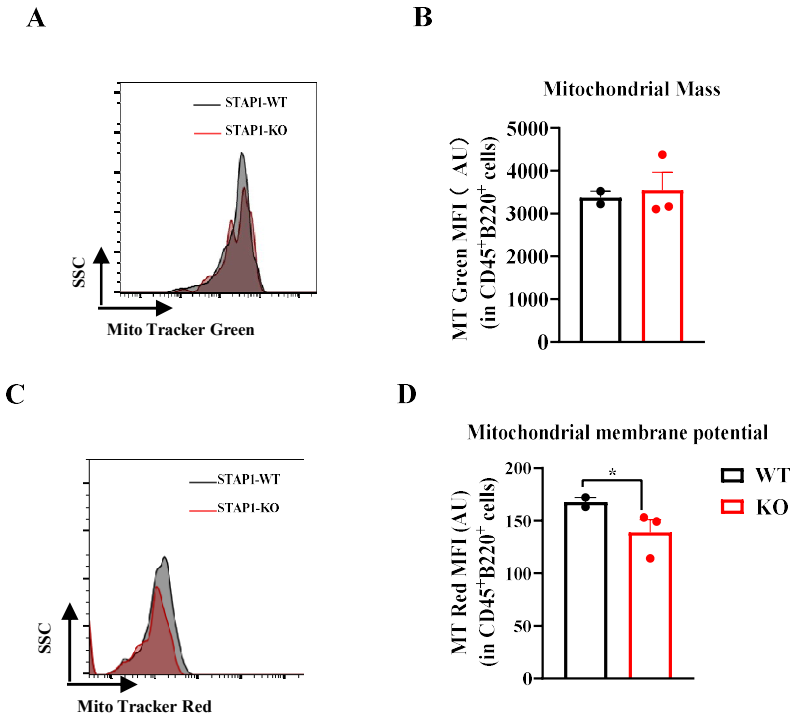

Figure 4.2.6 Ablation of STAP1 decreases mitochondria potential. CD19+ B cells were sorted from splenic cells of either STAP1-WT or STAP1-KO mice using anti-CD19 MicroBeads. Sorted B cells were stained with Mito Tracker Green and Mito Tracker Red, followed by flow cytometric analysis. The mitochondrial mass was assessed by Mito Tracker Green levels (A), which was quantified based on the mean fluorescence intensity (MFI) levels (B). The mitochondrial menbrane potential was assessed by Mito Tracker Red levels (C) with quantification (D). Data are expressed as mean ± SEM (n = 2-3). * $p < 0.05$; ** $p < 0.01$;*** $p < 0.001$. Each dot represents the measurement of an individual mouse and the column indicates the average.

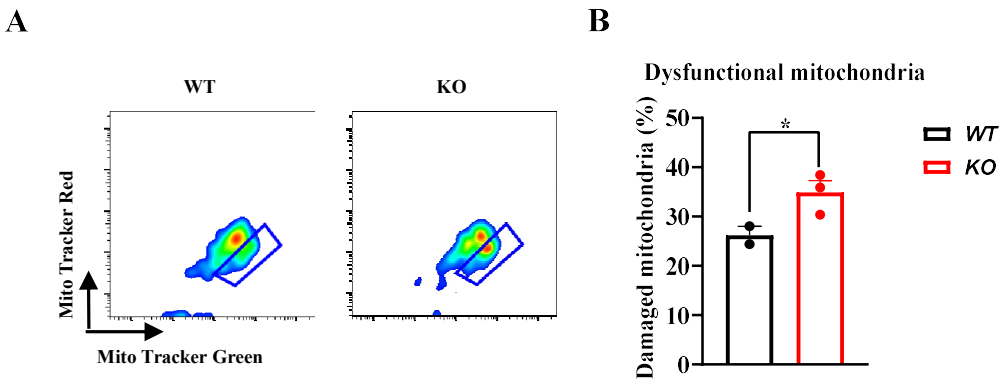

Figure 4.2.7 Lack of STAP1 leads to mitochondria dysfunction. $CD19^{+}$ B cells were sorted from splenic cells of either STAP1-WT or STAP1-KO mice using anti-CD19 MicroBeads. Sorted B cells were stained with Mito Tracker Green and Mito Tracker Red, followed by flow cytometric analysis. Cells with dysfuncitonal mitochondria were revealed as Mito Tracker $Green^{high}$Mito Tracker Red^{low} (A) with quntification (B). Data are expressed as mean ± SEM (n = 2-3). * $p < 0.05$; ** $p < 0.01$;*** $p < 0.001$. Each dot represents the measurement of an individual mouse and the column indicates the average.

To explore why primary splenic B cells from STAP1-KO mice had more dysfunctional mitochondria, these cells were checked by the number of mitochondria or the biogenesis of mitochondria by RT-qPCR. Similar to the data with knockdown STAP1 in the hybridoma B cell model, there was no significant change in the number of mitochondrial DNA between the three groups (Figure 4.2.8 A). Next, I also checked the biogenesis of mitochondria, including mitochondrial transcription factor A (TFAM), NADH-ubiquinone oxidoreductase

chain five protein (mtND5) (complex I), cytochrome b (CYTB) (complex III), and cytochrome oxidase III (COXIII) （complex IV). Decreasing mRNA expression levels of TFAM, mtND5, CYTB, and COXIII were discovered in sorted B cells of STAP1-KO mice, compared with their controls (Figure 4.2.8 B-E). Except for the mRNA expression level, the protein level of mitochondrial complexes in these cells was also quantified by western blotting. The protein expression of complex I and complex IV in mitochondria of primary splenic B cells from STAP1-KO mice revealed lower protein expression levels, compared with their controls (Figure 4.2.9 A and B).

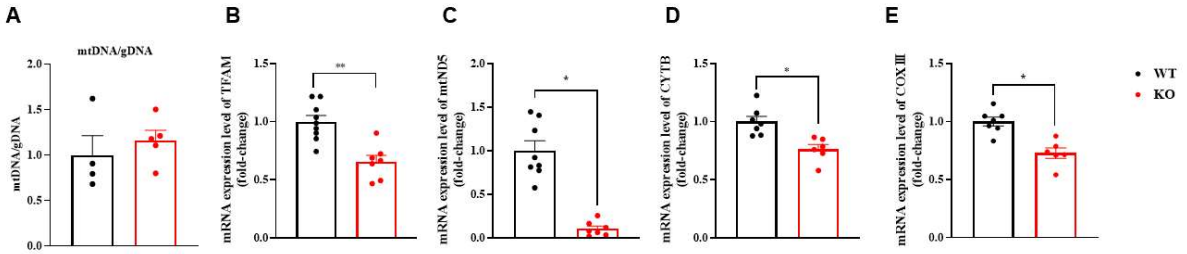

Figure 4.2.8 Deletion of STAP1 reduces the mRNA expression of mitochondrial biogenesis. CD19^{+} B cells were isolated from splenic single cells of either STAP1-WT or STAP1-KO mice using anti-CD19 MicroBeads. Cells were collected for RNA extraction, and qPCR was conducted to determine the mRNA expression level of mitochondrial DNA (mtDNA) normalized with genomic DNA (gDNA) (A) and determined the mRNA expression level of mitochondrial biogenesis genes, Mitochondrial transcription factor A (TFAM) (B), NADH-ubiquinone oxidoreductase chain five protein (mtND5) (complex I) (C), cytochrome b (CYTB) (complex III) (D), and cytochrome oxidase III (COXIII) （complex IV) (E). Data are expressed as mean ± SEM (n = 7 - 8). * $p < 0.05$; ** $p < 0.01$;*** $p < 0.001$. Each dot represents the measurement of an individual mouse and the column indicates the average.

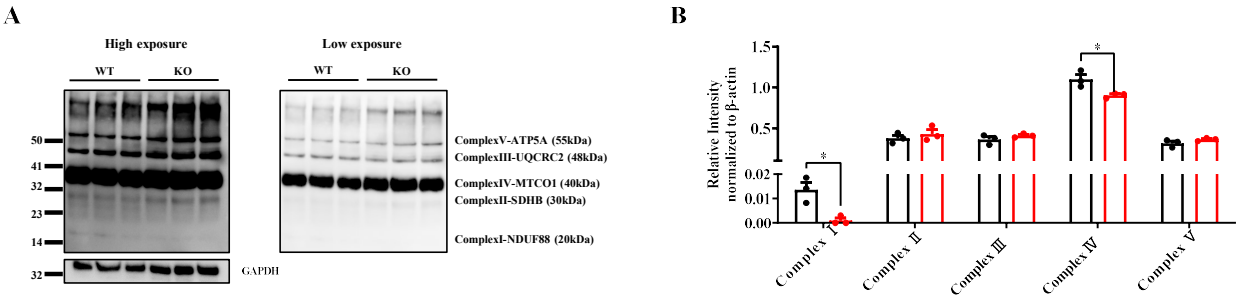

Figure 4.2.9. Mitochondrial damage in the ablation of STAP1 causes decreasing mitochondrial complex. CD19^{+} B cells were sorted from splenic cells of either STAP1-WT or STAP1-KO mice using anti-CD19 MicroBeads. The protein expression levels of mitochondrial complexes in sorted B cells were determined using western blot (A) with quantification (B). Data are expressed as mean ± SEM (n =3). * $p < 0.05$; ** $p < 0.01$;*** $p < 0.001$. Each dot represents the measurement of an individual mouse and the column indicates the average.

4.2.5 Elimination of STAP1 generates more superoxide

MitoSox is a permeant probe for alive cells with the cationic triphenylphosphonium substituent, the positive amount of this molecule allows the utilization of the probe by aggressively respiring mitochondria. Once the probe gets inside the mitochondria, another element of MitoSOX, dihydroethidium, can be oxidized by superoxide creating the 2-hydroxyethidium, which reveals a fluorescence excitation, representing the mitochondrial reactive oxygen species (ROS) production. ROS production emphasizes oxidative damage and can induce mitochondrial dysfunction[70-71].

The higher mean fluorescence intensity (MFI) of MitoSox was detected among primary splenic B cells from STAP1-KO mice, compared with their controls (Figure 4.2.10 B). That implicated primary splenic B cells from STAP1-KO mice had a larger number of dysfunctional mitochondria, which was reliable with the data of staining with MitoTracker Red.

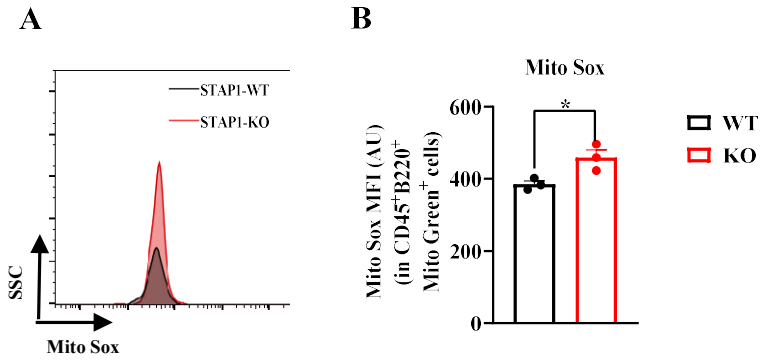

Figure 4.2.10 Elimination of STAP1 generates more superoxide. $CD19^+$ B cells were sorted from splenic cells of either STAP1-WT or STAP1-KO mice using anti-CD19 MicroBeads. Sorted B cells were staied with Mito Sox for assessing mitochondrial superoxide production using flow cytometry (A) with quantification (B). Data are expressed as mean ± SEM (n = 2-3). * $p < 0.05$; ** $p < 0.01$;*** $p < 0.001$. Each dot represents the measurement of an individual mouse and the column indicates the average.

4.2.6 Overexpressing STAP1 improves mitochondrial respiration and glycolysis

Except for the studies on the knockdown STAP1 cell model, I examined the mitochondrial function using the Seahorse Extracellular Flux Analyzer with primary splenic B cells from B cell specific overexpressing STAP1 mice. In contrast to the knockdown model, the B cell specific overexpressing STAP1 showed a sustained improvement in OCR after FCCP injection, compared with their controls (Figure 4.2.11 A). Increasing levels of maximal respiration (Figure 4.2.11 B), ATP production (Figure 4.2.11 C), and spare respiration capacity (Figure 4.2.11 D) were shown in the primary splenic B cells from B cell specific over expressing STAP1 mice. In the glycolysis stress test, the primary splenic B cells from B cell specific over expressing STAP1 mice revealed a raising in ECAR (Figure 4.2.12 A), glycolysis (Figure 4.2.12 B), glycolysis capability (Figure 4.2.12 C) after glucose and oligomycin injection and glycolysis reserve (Figure 4.2.12 D).

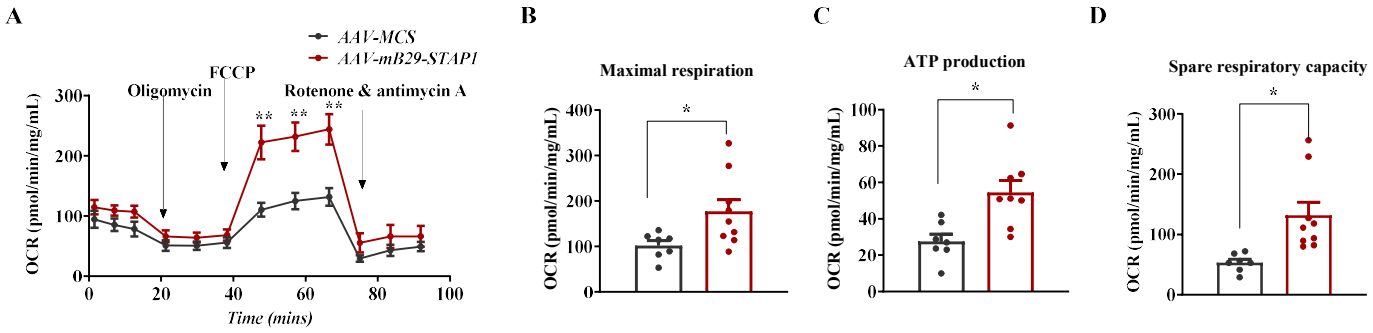

Figure 4.2.11 Specific B cell over expressing STAP1 improves mitochondrial respiration. 8-wee -old mice were intraperitoneally injected with AAV-mB29-STAP1 or its corresponding controls AAV-MSC. $CD19^+$ B cells were isolated from splenic single cells of either AAV-mB29-STAP1 or AAV-MSC mice using anti-CD19 MicroBeads. The oxygen consumption rates (OCR) were measured using the Aligent Seahorse XF Cell Mito Stress test (A), and the maximal respiration (B), ATP production (C) and spare respiratory capacity (D) of mitochondrial OCR were assessed. Data are expressed as mean ± SEM (n = 9-10). * $p < 0.05$; ** $p < 0.01$;*** $p < 0.001$. Each dot represents the measurement of an individual mouse and the column indicates the average.

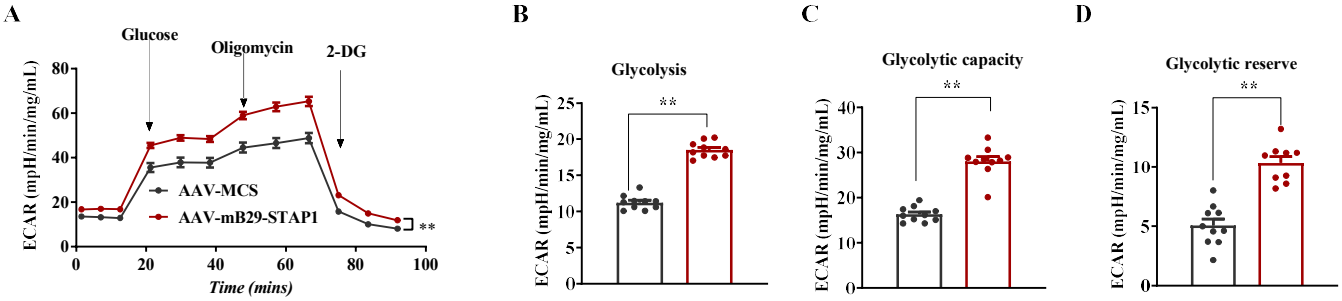

Figure 4.2.12 Specific B cell over expressing STAP1 enhances the ability of glycolysis. 8-week-old mice were intraperitoneally injected with AAV-mB29-STAP1 or its corresponding controls AAV-MSC. $CD19^+$ B cells were isolated from splenic single cells of either AAV-mB29-STAP1 or AAV-MSC mice using anti-CD19 MicroBeads. The extracellular acidification rates (ECAR) were measured using the Seahorse analysis (A), and glycolysis (B), glycolytic capacity (C) and glycolytic reserve (D) were quantified. Data are expressed as mean ± SEM (n = 9-10). * $p < 0.05$; ** $p < 0.01$;*** $p < 0.001$. Each dot represents the measurement of an individual mouse and the column indicates the average.

4.2.7 STAP1 binds to prohibitins

Previous studies demonstrated that STAP1 is positive regulation of BCR signalling pathway and BCR signalling is essential for B cell antibody production[72] , but molecular mechanisms by which STAP1 regulating the B cell primary antibody production remain to be fully elucidated. I performed TAP-tag pull down to explore the function of STAP1 via its binding proteins by mass spectrometry. In brief, many mitochondrial proteins were pulled down by TAP-tag STAP1 but not control (Table 4.2.1). Interestingly, various databases suggested that STAP1 protein can be detected in mitochondria. Amount the mitochondrial proteins, we are interested in the interaction of STAP1 and prohibitin 1 (PHB) and 2 (PHB2). prohibitins (PHBs) are ubiquitously expressed protein that play an important role on mitochondrial functions including mitochondrial biogenesis and oxidative phosphorylation[73]. Therefore, we performed co-immunoprecipitation to verify the binding between STAP1 and PHB (Figure 4.2.13 A). Interestingly, we found that the expression level of PHB proteins in the B cells of STAP1 KO mice were significantly lower than their WT controls (Figure 4.2.13 B and C).

Table 4.2.1 List of mitochondrial proteins pulled down by TAP-tagged STAP1. The matching results of purified protein from HEK293 transfected with TAP-tagged STAP1 or negative control cell were compared. Only those that were presented in matching results of HEK293 transfected with TAP-tagged STAP1 protein are listed. The matched proteins are presented in descending order of confidence level.

Accession	Description	Mascot Protein Score	Protein Molecular Mass	Total significant sequence matched	Significant unique sequence matched	Sequence coverage (%)
STAP1	Signal-transducing adaptor protein 1	205	34498	8	8	51
PHB	Prohibitin	324	29843	7	7	38
VDAC1	Voltage-dependent anion-selective channel protein 1	286	30868	7	7	34
VDAC2	Voltage-dependent anion-selective channel protein 2	194	32060	5	5	32
NDUA4	Cytochrome c oxidase subunit NDUFA4	50	9421	2	2	27
HS71A	Heat shock 70 kDa protein 1A	207	70294	7	5	17
PYC	Pyruvate carboxylase, mitochondrial	715	130293	12	12	16

SFXN1	Sideroflexin -1	60	35881	2	2	15
RAP1A	Ras-related protein Rap-1A	57	21316	2	2	15
ADT2	ADP/ATP translocase 2	213	33059	4	1	14
ADT3	ADP/ATP translocase 3	208	33073	4	1	14
CH60	60 kDa heat shock protein, mitochondrial	193	61187	4	4	12
PHB2	Prohibitin-2	170	33276	2	2	11

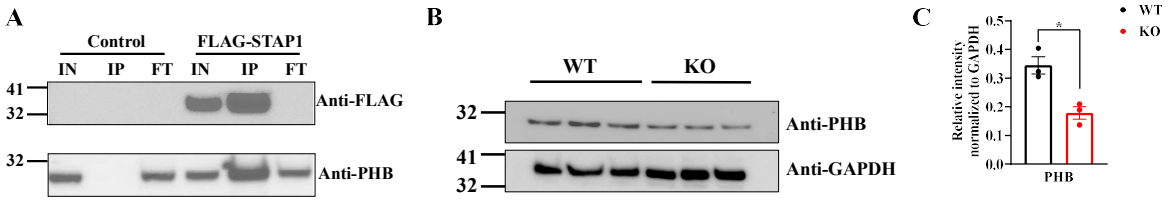

Figure 4.2.13 STAP1 binds to prohibitin. (A) Cell lysates were prepared from the 293T cell line which overexpressed STAP1 followed by co-immunoprecipitaion using anti-FLAG to confirm the protein interaction between STAP1 and PHB. (B-C) B cells were sorted from the spleen of 8-week-old STAP1-WT or STAP1-KO mice using anti-CD19 MicroBeads. Cell-associated PHB was measured by western blot (B) and the bands were quantified (C). Data are expressed as mean ± SEM (n = 3). * $p < 0.05$; ** $p < 0.01$;*** $p < 0.001$. Each dot represents the measurement of an individual mouse and the column indicates the average.

4.3 Summary

Recently, researchers who are mainly focused on immunology started to transfer their concern on how the cell-based metabolism of immune cells influence immune response. High energy is needed for immune cells to activate their immune response. Moreover, germinal centre B cells generats antibodies, supported by the energy from mitochondrial respiration and glycolysis [16-17]. Therefore, studying the metabolism of B cells with or without STAP1 expression may justify how STAP1 regulated immune response.

In this chapter, I designed the experiment mainly employing Seahorse Extracellular Flux Analyzer and MitoTracker staining to determine the function of mitochondria in different models, including primary B cells from STAP1-KO mice or B cell specific over expressing STAP1 mice, and hybridoma B cells transfected with siRNA-STAP1. The results were consistent. In knockdown or knockout of STAP1 models, weaker mitochondrial respiration and glycolysis were detected. While improved mitochondrial respiration and glycolysis were exhibited in primary B cells from B cell specific over expressing STAP1 mice. In Mitotracker staining, primary B cells from STAP1-KO mice had more dysfunctional mitochondria but did not change the number of mitochondria, compared with their controls. Likewise,

in primary B cells from STAP1-KO mice or hybridoma B cells transfected with si-RNA-STAP1, there was less mRNA expression of mitochondrial biogenesis and no change in the number of mitochondria. As previous studies demonstrated that PHBs physically interact with mitochondrial complex I in human cells and might play a role in the assembly or degradation of mitochondrial complex I[74-75]. By immunoblotting for molecular markers of the mitochondrial respiratory chain complexes, downregulations of complex I in STAP1-KO splenic B cells was confirmed. Additional, the binding between STAP1 and PHB was verified by co-immunoprecipitation and lower expression level of PHB proteins in the B cells of STAP1-KO mice were found. Together, these data indicate that STAP1 is required in the maintenance of mitochondrial function in B cells.

Chapter 5- Hepatic homeostasis required expression of STAP1

5 Hepatic homeostasis requires expression of STAP1

5.1 Introduction

STAP1 was widely reported as the fourth causative gene of hypercholesterolemia in the past decades[26-27, 39-40, 53]. The reason behind this was that many research groups revealed lots of variants of STAP1 in hypercholesterolemia patients or patients' families, compared with healthy individuals, via scanning genomic DNA sequencing. With more and more studies on this topic published, inconsistent reports were released indicating that there might be no association between STAP1 mutation and hypercholesterolemia. It was reported that individuals carrying the STAP1 variants were stable at a healthy level of serum cholesterol level[41]. Besides, the variants which were supposed to be damaged might not affect the serum cholesterol change by different methods of analysis [43, 50]. In addition, two research groups mainly paid attention to the metabolism change using the STAP1 global knockout mouse model. Based on their result, there was no difference in metabolic parameters, including blood random or fasting glucose, serum cholesterol level, and serum triglyceride level[44-45]. The global STAP1-KO mouse model they used was the same knockout strategy as mine. Consequently, to summarize the results of all these studies, STAP1 was first supposed as the fourth causative gene of

hypercholesterolemia in the clinical report by finding STAP1 variants in hypercholesterolemia patients. Secondly, with increasing studies on the different STAP1 variants, researchers found that not all the variants were linked with inducing hypercholesterolemia. The reason might owe that there were large numbers of STAP1 variants located on different positions of *the* STAP1 gene. Moreover, the experimental assay using a knockout mouse model mainly measured the phenotype without gene STAP1 expression, which was studying the change in the loss of STAP1 function under the hypothesis that STAP1 variants impaired the STAP1 protein function. But gene mutation did not only mean losing the protein function that its codes. Against this, there might encode a new protein by STAP1 variants to regulate other functions, inducing hypercholesterolemia.

Therefore, in this chapter, I planned to check the phenotype related to hypercholesterolemia using a B cell specific overexpressing STAP1 mouse model via an adeno-associated virus system, which was a different model from the STAP1 global knockout mouse model. Meanwhile, I noticed the research group that was using the same knockout mice as mine, feeding mice with a western diet (42%kcal) but got no significant difference in metabolic change. Hence, I also proposed to feed the STAP1-KO mice with a high-fat diet (62%kcal), which with

higher calories than before to further confirm the relationship between deficiency of STAP1 and hypercholesterolemia.

5.2 Result

5.2.1 *STAP1* greatly induces in the liver of high-fat diet feeding

To study the connection between STAP1 and familial hypercholesterolemia, 8-week-old mice were fed a high-fat diet (HFD) to construct the non-alcoholic fatty liver disease model, and mice were fed with a standard chow diet (STC) as a control. After 12 weeks of feeding, the HFD mice and their corresponding control littermates were sacrificed and their spleens were collected for RT-qPCR and western blot. Intriguingly, STAP1 greatly induces in the liver after high-fat diet feeding (Figure 5.2.1 A). Single cells were isolated from the liver and purified by the $CD19^+$ Microbeads to get the hepatic B cells. The data shows that the induction of STAP1 after HFD feeding occurred in the hepatic B cells instead of hepatocytes (Figure 5.2.1 B). To further understand whether the frequenccy of B cells change or not after HFD treatment, single cells isolated from these three tissues was stained with anti-CD19, followed by flow cytometry (Figure 5.2.2 A). The result indicates that there is no significant change between STC and HFD (Figure 5.2.2 B).

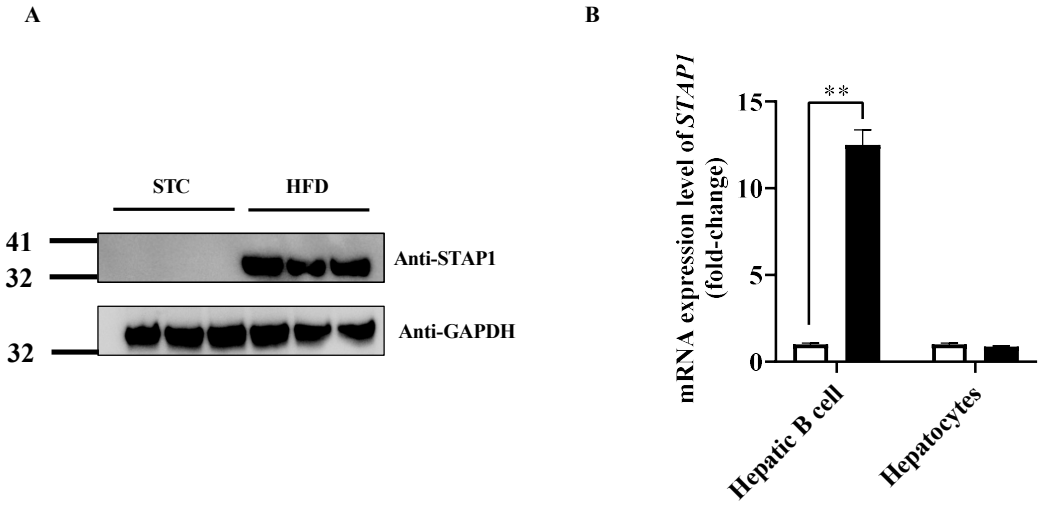

Figure 5.2.1 STAP1 greatly induces in the liver of high-fat diet feeding. Wildtype mice upon standard chow feeding or after 12-week high-fat diet feeding were sacrificed for liver collection. RT-qPCR and western blot were performed to quantify the m RNA and protein expression level of STAP1. Protein (A) and mRNA (B) expression levels in the liver under STC and HFD feeding were quantified. Data are expressed as mean ± SEM, * indicated a significant difference, *$p < 0.05$; **$p < 0.01$; ***$p < 0.001$ (n=3). Each dot represents the measurement of an individual mouse, and the column indicates the average.

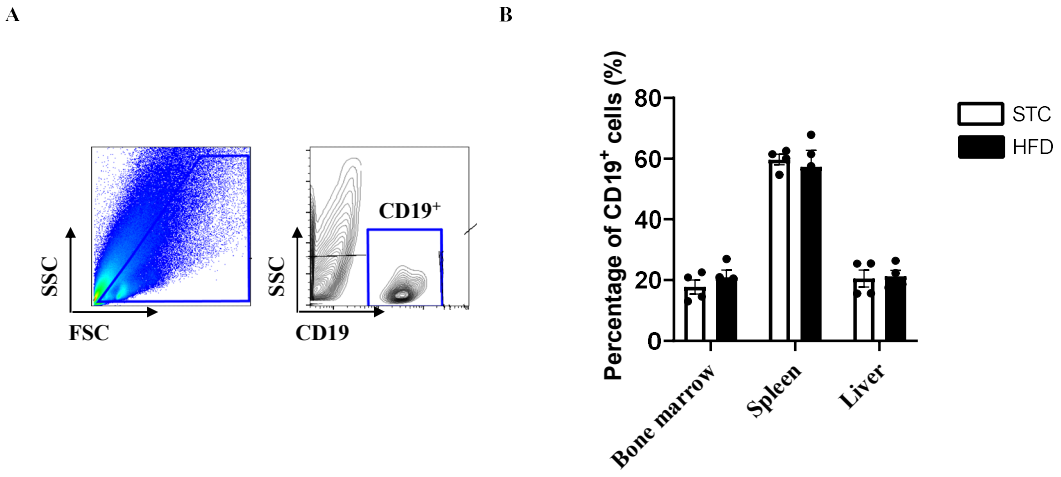

Figure 5.2.2 STAP1 does not affect the population of B cells after high-fat diet feeding. Wildtype mice upon standard chow feeding or after 12-week high-fat diet feeding were sacrificed for bone marrow, spleen, and liver collection. Followed by flow cytometry to measure the B cell population (A). Quantification of the frequencies of B cells in various tissue after high-fat diet feeding, compared with standard chow feeding (B). Data are expressed as mean ± SEM, * indicated a significant difference, *$p < 0.05$; **$p < 0.01$; ***$p < 0.001$ (n=4). Each dot represents the measurement of an individual mouse, and the column indicates the average.

5.2.3 *STAP1* deficiency increases serum triglyceride and total cholesterol after fasting under STC feeding

For investigating how STAP1 regulated hepatic function, baseline characteristics on the STC diet were assessed at the age of 8 weeks randomly or after fasting for 16 hours. Similar body weight (Figure 5.2.3 A), blood glucose (Figure 5.2.3 B), triglyceride (Figure 5.2.3 C), serum total cholesterol (Figure 5.2.3 D) between STAP1-WT and STAP1-KO mice were found randomly. And there were no differences in body weight (Figure 5.2.3 A), blood glucose (Figure 5.2.3 B) between STAP1-WT and STAP1-KO mice after fasting. Interestingly, higher triglyceride (Figure 3.2.3 C), serum total cholesterol (Figure 3.2.3 D) levels were observed after 16 hours of fasting in STAP1-KO mice, compared with their STAP1-WT littermates. We checked whether deletion of STAP1 would also reduce their cytokine production. Then, we checked the production of cytokines from their splenic B cells. Notably, the anti-inflammatory cytokine IL-10 produced by the splenic B cells dramatically was decreased that isolated from STAP1-KO mice as compared to their STAP1-WT controls (Figure 3.2.4).

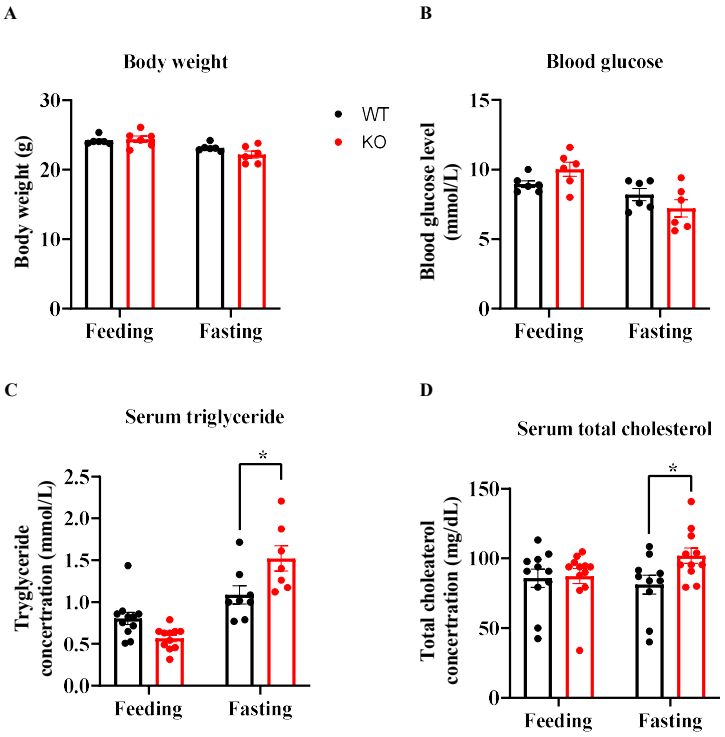

Figure 5.2.3 STAP1 deficiency increases serum triglyceride and total cholesterol after 16 hours of fasting under STC feeding. Basic metabolic parameters of STAP1 KO and their WT littermates were measured randomly or after 16 hours of fasting, including body weight (A), blood glucose (B), serum triglyceride (C), serum total cholesterol(D). Data are expressed as mean ± SEM. *indicated a significant difference, *$p < 0.05$; **$p < 0.01$; ***$p < 0.001$ (n=10-12). Each dot represents the measurement of an individual mouse, and the column indicates the average.

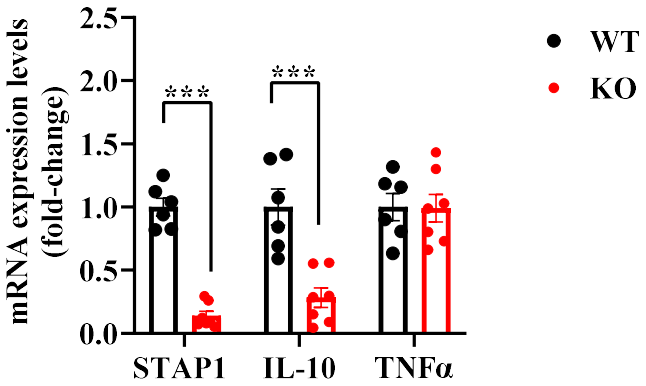

Figure 5.2.4 STAP1 deficiency decreases Il-10 mRNA expression. Sorted splenic B cells were used for RT-qPCR to quantify the expression level of IL-10 and TNFα. Data are expressed as mean ± SEM. *indicated a significant difference, *$p < 0.05$; **$p < 0.01$; ***$p < 0.001$ (n=7-8). Each dot represents the measurement of an individual mouse, and the column indicates the average.

5.2.4 Specific B cells overexpressed STAP1 improves glucose homeostasis after HFD feeding

To study the relationship between STAP1 and hepatic function, a B cell specific expressed STAP1 mouse model was applied for the experiment. The reason why not learned more about STAP1-KO mice was that researchers who used the same knockout mouse model, had already reported there were no changes in the baseline measurements of metabolism no matter under the STC diet or western diet even after 16 weeks. As Kanuri indicated, all these experiments, based on the same STAP1-KO mice, were generally regarded as a loss of function model, and could not get any clues about the connection between STAP1 expression and hepatic homeostasis. In another word, if the relation of STAP1 to hypercholesterolemia was owing to lacking STAP1 but obtaining a new function, that meant the missense mutation on STAP1 may translate into another potential functional protein to break the balance in hepatic homeostasis.

Hence, 8-week-old STAP1-WT mice were injected intraperitoneally with AAV-mB29-STAP1 and its corresponding control AAV-MCS separately. mB29 is a B cell specific promoter that drives STAP1 expressing particularly in B cells. Verifying whether the associated-adeno virus worked or not, after 8-week injection,

purified B cells and non-B cells using $CD19^+$ Microbeads isolation kit from the spleen of overexpressed mice and their corresponding controls were applied for total RNA extraction and protein lysate. RT-qPCR was performed to quantify the mRNA expression level of B cells and non-B cells from the spleen, and western blotting was conducted to measure the protein expression. Compared with the controls, higher STAP1 mRNA expression (Figure 5.2.5 A) and protein expression level (Figure 5.2.5 B) were found in splenic B cells from AAV-mB29-STAP1 mice, while there were no different changes in non-B cells between the two groups. That was suggesting the STAP1 overexpressed mouse model targeting B cells was successfully constructed. However, no noticeable changes were observed after injection under STC feeding, including body weight (Figure 5.2.5 C), random feeding blood glucose or glucose fasting after 16 hours (Figure 5.2.5 D), serum triglyceride (Figure 5.2.5 E) and total cholesterol (Figure 5.2.5 F).

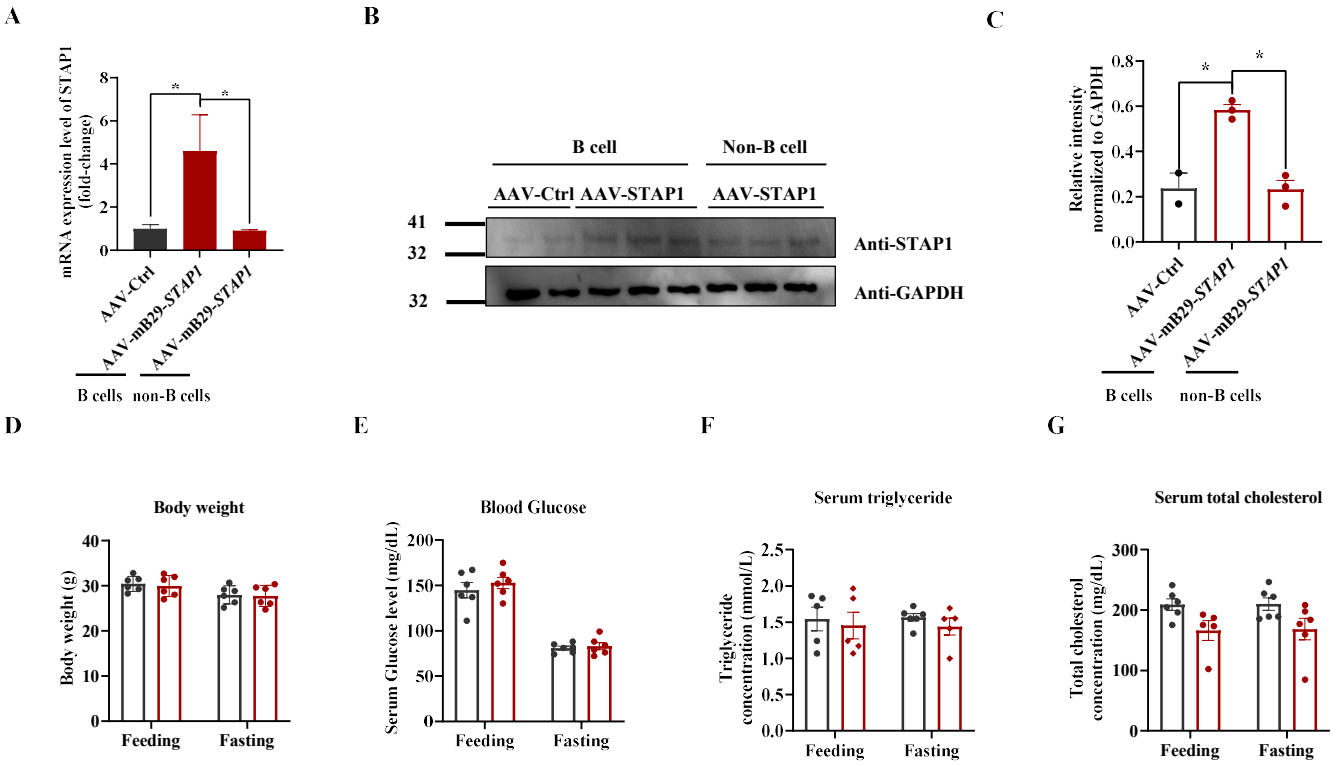

Figure 5.2.5 STAP1 B cell specific overexpressing mice has no change in the metabolism upon STC feeding. 8-week-old wildtype mice were injected intraretinally with AAV-mB29–STAP1 and their corresponding control AAV-MCS separately. Splenic isolated B cells were measured the m RNA expression (A) and protein expression (B and C) of STAP1 by RT-qPCR and western blotting. Followed by basal metabolic parameters were measured randomly upon feeding or after 16 hours of fasting, including body weight (D), blood glucose (E), serum triglyceride (F), serum total cholesterol (G). Data are expressed as mean ± SEM. *indicated a significant difference, *$p < 0.05$; **$p < 0.01$; ***$p < 0.001$ (n=6). Each dot represents the measurement of an individual mouse, and the column indicates the average.

Therefore, we fed the overexpressed mice with HFD, to learn more about the connection between STAP1 and hypercholesterolemia. We checked the basic metabolic parameters every four weeks after HFD treatment. Nevertheless, there was no significant change in body weight (Figure 5.2.6 A), random feeding blood glucose (Figure 5.2.6 C), fasting and feeding serum triglyceride (Figure 5.2.6 D, E). Interestingly, fasting glucose significantly decreased discovered on weeks 4, 8, and 12 after HFD treatment (Figure 5.2.7 B). Besides, B cells specific overexpressed STAP1 mice resulted in reducing fasting and feeding serum total cholesterol at weeks 4, 8, and 12 after HFD treatment (Figure 5.2.7 A and B) and lessened the fasting serum LDL-C levels at the 4^{th}, $8^{th,}$ and 12^{th} week (Figure 5.2.7 C), feeding serum LDL-C level at the week of 4 (Figure 5.2.7 D). In addition, no change was found in the fasting and feeding serum HDL-C (Figure 5.2.7 E and F).

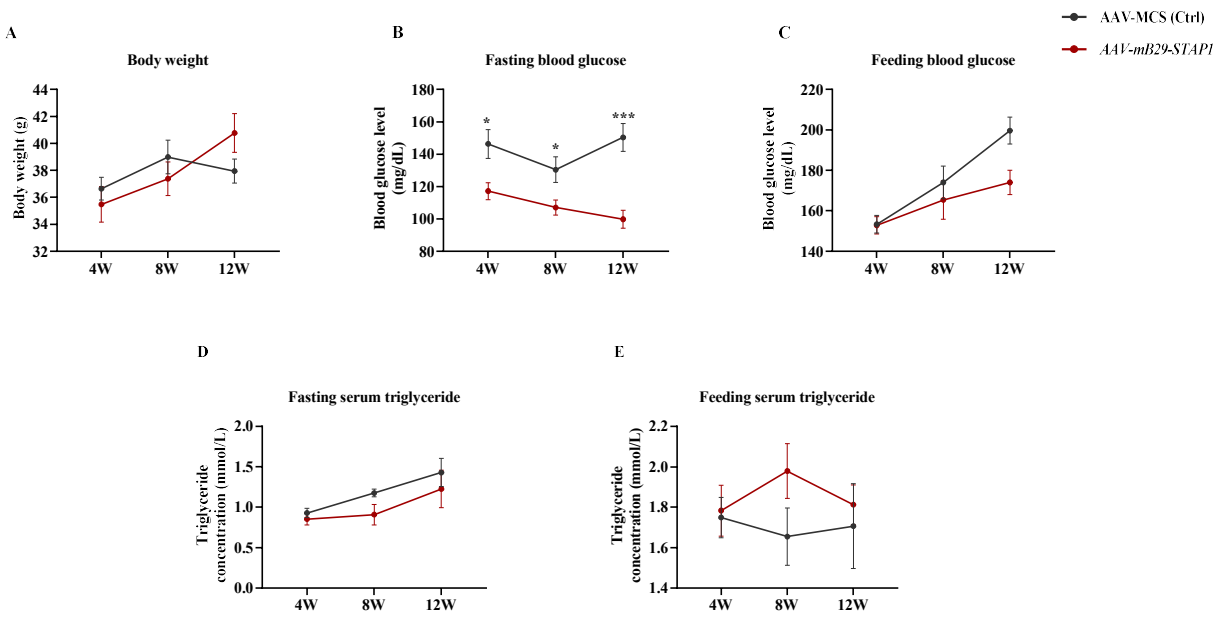

Figure 5.2.6* STAP1 *B cell specific overexpressing mice has no change in body weight, random or fasting glucose, and serum triglyceride under HFD feeding. 8-week-old wildtype mice were injected intraretinally with AAV-mB29–STAP1 and their corresponding control AAV-MCS separately. High-fat diet was treated after 8 weeks of injection, basal metabolic parameters were measured every 4 weeks randomly upon feeding or after 16 hours of fasting, including body weight (A), blood glucose (B and C), serum triglyceride (D and E). Data are expressed as mean ± SEM. *indicated a significant difference, *$p < 0.05$; **$p < 0.01$; ***$p < 0.001$ (n=6). Each dot represents the measurement of an individual mouse, and the column indicates the average.

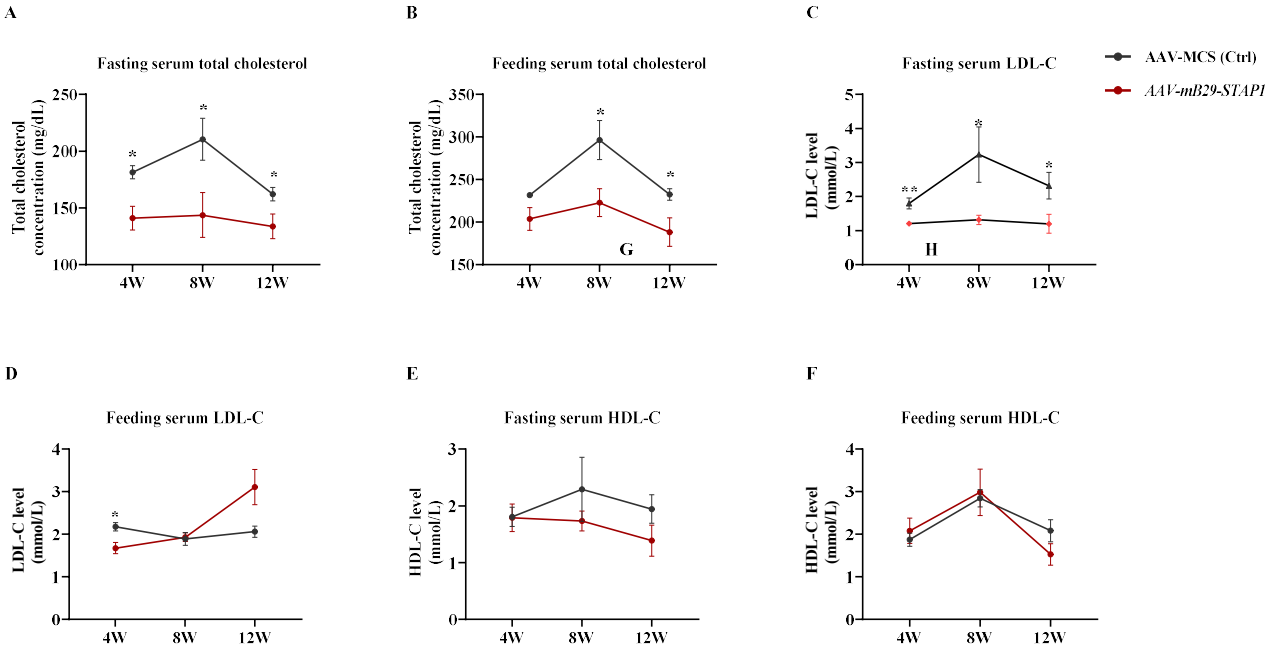

Figure 5.2.7 STAP1 B cell specific overexpressing mice show lower serum total cholesterol and LDL-C under HFD feeding. 8-week-old wildtype mice were injected intraretinally with AAV-mB29–STAP1 and their corresponding control AAV-MCS separately. High-fat diet was treated after 8 weeks of injection, basal metabolic parameters were measured every 4 weeks randomly upon feeding or after 16 hours of fasting, including serum total cholesterol (A and B), serum LDL-C (C and D), serum HDL-C (E and F). Data are expressed as mean ± SEM. *indicated a significant difference, *$p < 0.05$; **$p < 0.01$; ***$p < 0.001$ (n=6). Each dot represents the measurement of an individual mouse, and the column indicates the average.

Owing to the multiple phenotypes of the STAP1 overexpressed mouse model, a glucose tolerance test was performed to further assess glucose homeostasis in mice. Glucose was injected intraperitoneally with a dosage of 1.5g/kg after 16 hours of fasting for the glucose tolerance test. The result showed that glucose clearance significantly increases as evidenced by a downregulation of AUC (Figure 5.2.8 A and B). On the other hand, blood glucose was measured after insulin injection at the dose of 0.75 IU/kg for the insulin tolerance test. Mice were fasted 6 hours before an insulin injection. The data indicated that insulin sensitivity slightly enhanced in B cells specific overexpressed STAP1 mice (Figure 5.2.8 C and D). In addition, 2g/kg pyruvate was intraperitoneally injected after 16 hours of fasting. Surprisingly, gluconeogenesis diminished in AAV-mB19-STAP1 mice as demonstrating by the decline in the AUC (Figure 5.2.8 E and F).

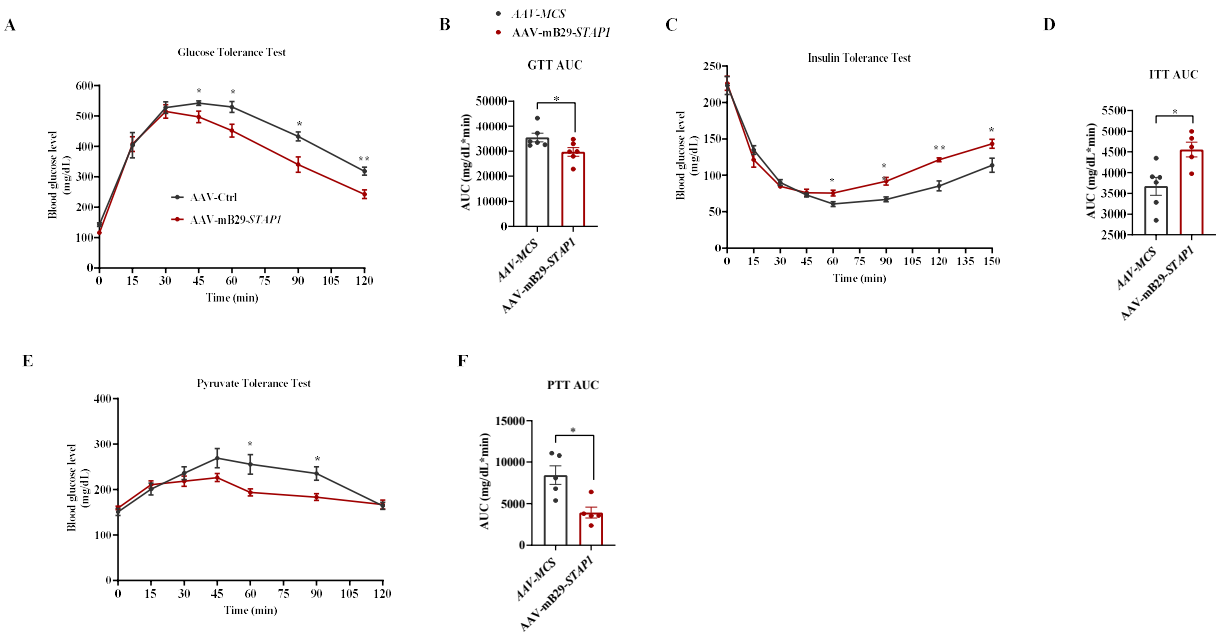

Figure 5.2.8 STAP1 B cell specific expressing affected glucose homeostasis in mice. 8-week-old wildtype mice were injected intraretinally with AAV-mB29–STAP1 and their corresponding control AAV-MCS separately. High-fat diet was treated after 8 weeks of injection. Followed by glucose tolerance test (GTT) (A), insulin tolerance test (ITT) (C), and pyruvate tolerance test (PTT) (E) was conducted 4 weeks after HFD feeding. The area under the curve (AUC) of GTT (B), ITT (D), and PTT (F) are calculated. Data are expressed as mean ± SEM. *indicated a significant difference, *p < 0.05; **p < 0.01; ***p < 0.001 (n=6). Each dot represents the measurement of an individual mouse, and the column indicates the average.

5.3 Summary

Familial hypercholesterolemia is a common genetic disease mainly caused by the mutation of LDLR, APOB, and PCSK9. STAP1, expressed in the immune cell, is supposed to be the fourth causative gene. But it is highly controversial, recent studies indicate that STAP1 has no connection with FH. It is well known that STAP1 is mainly expressed in the spleen, but its function is remained to be explored. Refer to the inconsistent studies, except for confirming again the metabolic parameters change using the STAP1-KO mice model. I constructed a B cell specific over expressing STAP1 mouse model to make it clear whether STAP1 expression was required to maintain glucose homeostasis.

In this chapter, I found that lack of STAP1 increased serum cholesterol and triglyceride after fasting. Additionally, in the B cell specific over expressing STAP1 mouse model, glucose homeostasis had been enhanced after high-fat diet feeding, including the capability of glucose clearance, insulin sensitivity, and hepatic gluconeogenesis, which proved that STAP1 was required for sustaining glucose homeostasis.

Interestingly, the results I found in the STAP1-KO mice were different from the published studies. Compared with the mouse model used in the former studies, in the Loaiza group, their STAP1-KO mice are constructed based on the deletion of 5bp on the exon 3[44], while my STAP1-KO mouse model is designed on the obliteration of exon 5 with loxP site. The different locations of these two knockout mouse models may cause these different consequences. Therefore, more experiments need to be done to know more about the mechanism of how STAP1 exactly functions on glucose homeostasis maintenance.

Besides, to answer the question of why there are so many STAP1 variants that have different effects on inducing hypercholesterolemia, I hypothesized that maybe the variants did not cause the gain of function of STAP1 instead of loss of function. Which meant the mutant of STAP1 translated into a new functional protein, in which impaired glucose homeostasis. In another word, the stable expression of STAP1 was required for providing glucose homeostasis, which could prevent missense translation. Thus, in this study, I changed the mouse model from a STAP1-KO mouse into a B cell specific overexpressing STAP1 mouse model, using the adeno-associated virus system, to better know the relationship between STAP1 and glucose homeostasis. In this mouse model, I chose to over expressed

STAP1 specifically in B cell, due to B cell was the most expression location of STAP1. After getting the basic metabolic parameters under standard chow feeding, I also fed the mice with a high-fat diet as a stimulator to induce non-alcohol fatty liver in mice. The results demonstrated that STAP1 was required for glucose homeostasis maintenance.

Chapter 6- Discussion

6 Discussion

6.1 STAP1 presents an immune regulation function

In a study of mRNA sequencing using the lungs of COVID-19 patients, STAP1 is listed in the first place of related genes[56], which shifts our attention to how STAP1 mediated the immune response. STAP1 is initially supposed to be an immune system regulator as the substrate of TEC, controlling the immune system by regulating the intracellular signaling mechanism.

To measure the ability to react to the immune response is to quantify the antibody subclass, including IgG, and IgA, which suggests the polarization of immune response caused by adjuvant. The two adjuvants I used in the immunization are efficient to improve the antibody subclass secretion, indicating the activation of B cells by the support under T helper cells[76].

One of my findings was that STAP1 deficiency showed a weaker response to immunity not via the activation of dendritic cells or T cells. The limitation of the design of the ex vivo assay was examined widely using splenic single cells, which were a mixture of immune cells, instead of specific to one cell subset to check the association between the weaker response with the activation of dendritic cells of T cells. Dendritic cells are accountable for starting antigen-induced immune

responses[77]. Moreover, single cells from STAP1-KO mice presented less population after bone marrow differentiation into dendritic cells, which implied the weaker immune response might be caused by the smaller number of dendritic cells capturing the antigens. And to detect the activation of T cells, only CD3 was used as the surface marker to check the proliferation after stimulation, which meant only the total T cells population was detected. One of the reasons why there was no change in the proliferation of T cells was that change happens in the amount of functional T cell subtypes instead of the total number of T cells, for example, Th1, and Th2.

Notably, the obliteration of STAP1 showed different reactions to immune responses at distinct timepoint after immunization. Especially at the timepoint of the 10^{th} day after the third immunization, there was no change in the serum IgG in STAP1-KO mice, but a significant decline in the serum IgG2c and BALF IgA. IgG2c subclass antibody is crucial to the proper explanation of the Th1 immune response [78], and Th1 cells are necessary for the host defence against intracellular pathogens [5, 79]. My finding showed that STAP1 deficiency always decreased the serum IgG2c secretion, indicating that STAP1 is more needed in the Th1 immune response, compared with the Th2 immune response. Thus, to better understand how

STAP1 regulates immune response, apart from studying the association between B cells and STAP1, the relationship among STAP1, dendritic cells, and T cells can also be one of the parts for investigation.

6.2 STAP1 regulates immune response via B cell cell-based mitochondrial metabolism

B lymphocytes have a high demand for energy to constitutively secrete antibodies after activation [80]. In this study, we used STAP1-deficient mice and hybridoma cells to gain insight into the biological role of STAP1 and explore the importance of the immune cell-specific gene STAP1 in B cell antibody production and energy metabolism. We found that STAP1 is highly expressed in B lymphocytes, and its deficiency does not change the B lymphocyte population in mice. Our findings are in agreement with recent publications showing that B lymphocyte populations are not altered in mice deficient in STAP1 [45] and carriers of STAP1 gene variants [44]. However, deletion of B lymphocyte STAP1 in mice results in the production of fewer antibodies, particularly upon first exposure to weak antigens. The antibody level of STAP1 KO mice is compatible with their WT littermates unless repeat exposures to strong antigens occur. We also found that STAP1 is required for optimal energy production in B lymphocytes during B cell activation.

BCR signalling is essential for B lymphocyte survival, development, and antibody production [81]. Previous studies have reported that STAP1 functions as a docking protein acting downstream of Tec (tyrosine kinase expressed in hepatocellular

carcinoma) tyrosine kinase in BCR signalling [36]. STAP1 is phosphorylated by Tec and participates in a positive feedback loop, increasing Tec activity [36]. Although tyrosine kinase plays an important role in B-cell development [82], Tec-deficient B lymphocytes isolated from Tec KO mice behave like wild-type cells in both in vitro proliferation assays and in vivo immunization experiments [83]. This lack of a major phenotypic alteration of the immune system is explained by the compensation effect of another tyrosine kinase, Bruton's tyrosine kinase (Btk), in murine B cells [83]. However, a follow-up study in 2017 demonstrated that Tec kinase limits the activating capacity of Btk, as supported by enhanced Tec-deficient B cell responses to model antigen and humoral immunity upon influenza infection [84]. Nevertheless, the phenotype of antibody production in Tec-deficient B cells is opposite to that of STAP1-deficient B cells. Therefore, we believe that B lymphocyte STAP1 regulates antibody production after vaccination via a Tec-independent pathway.

Previous studies have suggested that BCR signalling activates a B cell metabolic program [85]. Upon engaging antigen, B cells rapidly increase their metabolic activity, including both oxidative phosphorylation and glycolysis [85], but the detailed mechanism remains unclear. Previous studies have reported that cytokines stimulate the mitochondrial localization of tyrosine-phosphorylated signal

transducer and activator of transcription 5 (STAT5) in T cells [86], and mitochondrial STAT5 promotes the Warburg effect by inactivating the pyruvate dehydrogenase complex in cancer cells under hypoxic conditions [87]. Interestingly, STAP1 has been shown to interact with STAT5 by co-immunoprecipitation in HEK293T cells, and its ablation leads to the downregulation of antiapoptotic genes by impairing the phosphorylation status of STAT5 in chronic myeloid leukemia (CML) stem cells [48]. The interaction between STAP1 and STAT5 might explain the decrease in OCRs, but not the decrease in ECARs, in STAP1-deficient B cells and STAP1-knockdown hybridoma cells. Therefore, we believe that STAP1 regulates energy metabolism via other pathways.

Consequently, we performed an unbiased TAP-tagged pull-down assay to explore the function of STAP1 in antibody production and energy metabolism through its binding proteins. Interestingly, several mitochondrial proteins were pulled down, and we were particularly interested in the interaction between STAP1 and prohibitins (PHBs). PHBs are involved in many cellular processes such as cell-cycle progression, senescence, apoptosis, and particularly in the maintenance of mitochondrial function [88]. There are two PHB subunits named prohibitin 1 (PHB1)

and prohibitin 2 (PHB2). Both are ubiquitously expressed in many types of cells and are highly expressed in cells that heavily depend on mitochondrial function [89]. The interaction between STAP1 and PHBs provides an explanation for the phenotypes of B cells defective in STAP1, including disruption of complex I assembly, increased ROS production, and most importantly, a reduction in oxidative metabolism [90].

Membrane lipid rafts play important roles in B cell activation at multiple stages by controlling the local concentration of various receptors and regulatory molecules [45]. For example, lipid rafts serve as platforms for BCR signal transduction by regulating antigen presentation by membrane immunoglobulin M (mIgM) during B cell maturation [91-92]. Remarkably, PHBs can be found in most organelles [88]. Previous studies have reported the specific association of prohibitin with lipid rafts [93] and the IgM antigen receptor [94] of B cells. It would be interesting to further explore how STAP1 regulates the level of PHBs in cells by redistribution of PHBs at lipid rafts following by the activation of BCR signalling.

STAP1 has been suggested to be involved in leukemogenesis. High expression of STAP1 has been identified in B-cell acute lymphoblastic leukemia (B-ALL) [47]. However, high STAP1 expression levels were not found to be associated with poor five-year event-free survival, high measurable residual disease levels, or ex vivo resistance to chemotherapeutic drugs commonly used in B-ALL treatment [47]. Interestingly, a previous study found that STAP1 functions as an adaptor molecule downstream of c-kit in hematopoietic stem cells [38]. STAP1 expression is also aberrantly upregulated in chronic myeloid leukemia (CML) stem cells in patients' bone marrow, leading to downregulation of antiapoptotic genes and prolonging the survival of LSCs [48]. CML is a clonal disease characterized by the presence of an abnormal BCR-ABL fusion gene that activates multiple pathways involved in cell survival, growth promotion, and disease progression. STAP1 contributes to inducing proliferation in CML cells [49], making it a potential therapeutic target for CML, but not for B-ALL. Interestingly, overexpression of PHBs is associated with cancer, and inducing apoptosis by targeting PHBs has anti-tumour effects. [95]. It is interesting to further explore the interaction of STAP1 and PHBs influence CML cell proliferation and survival.

In summary, we utilized both loss- and gain-of-function experiments in mouse and cell models to investigate the role of B cell STAP1 on antibody production through energy metabolism reprogramming. Given that mouse and human STAP1 proteins share a high degree of sequence identity (83%) and similarity (90%) and have similar key domain regions, we believe that the findings from our mouse model could be extrapolated to humans, providing valuable insights into the function and role of STAP1 in antibody production.

6.3 STAP1 is the key to regulating the hepatic homeostasis

STAP1 is first reported as the fourth causative gene of hypercholesterolemia in 2014[26], even though it is mostly expressed in the immune cell but hardly found in the liver. The fourth gene as hypercholesterolemia is supposed when some hypercholesterolemia patients have some STAP1 variants. It drives many researchers to start performing sequencing with hypercholesterolemia patients and their families to confirm this fourth gene. Intriguingly, more and more STAP1 variants are found in hypercholesterolemia patients' families, when it comes to combining the variants with the functional validation studies, many individuals carrying these variants are unable to discover a role for STAP1 in regulating plasma lipid concentrations [41-43]. According to these negative findings, some investigators are supposed to exclude STAP1 as familial hypercholesterolemia.

Apart from the studies based on the sequencing database and clinical analysis, some research groups examine the hypothesis that deficiency of STAP1 can cause familial hypercholesterolemia using global STAP1-KO mice. Unfortunately, all these groups cannot find evidence to prove loss of STAP1 aggravates hypercholesterolemia. Moreover, there are also no significant changes in plasma lipids on the atherosclerosis plaque development in the transplant of STAP1

deficiency bone marrow into LDLR deletion mice[44]. A crucial limitation of these studies is missense STAP1 variants reported in humans can not be recapitulated by this loss of function model. In other words, it is hard to identify the STAP1 mutation intensifies hypercholesterolemia by losing the STAP1 protein function or gaining another new function via the protein translated by the missense variants.

It is worth noting that STAP1 is mainly expressed in immune cells. Some studies link STAP1 mutations with cardiovascular disease[40, 96]. Besides, immune cells had been associated with atherosclerosis and familial hypercholesterolemia[97]. STAP1 was originally known as the direct substrate of Tec, which is playing significant role in the immune system by regulating immune functions[35-36, 46]. There may be some hints to explain how the STAP1 variants affect lipid metabolism via immune cell function.

Therefore, I designed to learn the relationship between STAP1 and hypercholesterolemia using the B cell specific over overexpressing STAP1 to test whether STAP1 is essential for hepatic homeostasis. But more studies are needed to further uncover the STAP1 variants causing hypercholesterolemia.

In this study, I found STAP1 was needed for maintaining hepatic homeostasis, but the mechanism is still unknown. As STAP1 is mainly expressed in immune cells, learning the function of STAP1 in immune cells may be the key to answering the question. STAP1 deficiency mice show weaker immune response abilities due to dysfunctional mitochondria providing less energy. Thus, it is essential to make it clear whether STAP1 could regulate immune response via its metabolic function, which can provide some hints for figuring out the mechanisms behind some diseases. And it may also support novel therapeutic targets establishment for the treatment of diseases, in whom pathogenesis involved in abnormal B cells.

6.4 Future work

This research project only measured the lipid and glucose parameters in B cell specific overexpressing STAP1 mice, it was still a long way to explain the phenotype to clarify the association between STAP1 and hepatic homeostasis. Therefore, the mechanism behind this still needs to simplify by mRNA sequencing or other technology to explore the target gene or signaling to regulate hepatic homeostasis.

To investigate how STAP1 affects the immune response, studying whether STAP1 can mediate the proliferation or activation of dendritic cells and Th1 cells after stimulation is necessary. For further learning, whether the cell-based metabolism in STAP1 absence-B cells impairs the immune response, I should try to find more evidence to link these two elements. For example, give the energy back to the STAP1 absence-B cells to check whether they can secret the same level of the antibody as the STAP1 wild-type B cells. Furthermore, the mechanism of how STAP1 hinders the mitochondrial complex protein expression is also the key to supporting the link between STAP1 and immunometabolism.

6.5 Conclusion

In this study, I found STAP1 was needed for maintaining hepatic homeostasis, but the mechanism is still unknown. As STAP1 is mainly expressed in immune cells, learning the function of STAP1 in immune cells may be the key to answering the question. STAP1 deficiency mice show weaker immune response abilities due to dysfunctional mitochondria providing less energy. Thus, it is essential to make it clear whether STAP1 could regulate immune response via its metabolic function, which can provide some hints for figuring out the mechanisms behind some diseases. And it may also support novel therapeutic targets establishment for the treatment of diseases, in whom pathogenesis involved in abnormal B cells.

Chapter 7- References

1. Janeway, C. A., Jr.; Medzhitov, R., Innate immune recognition. *Annu Rev Immunol* **2002,** *20*, 197-216.

2. Netea, M. G.; Quintin, J.; van der Meer, J. W., Trained immunity: a memory for innate host defense. *Cell host & microbe* **2011,** *9* (5), 355-61.

3. Yatim, K. M.; Lakkis, F. G., A brief journey through the immune system. *Clinical journal of the American Society of Nephrology : CJASN* **2015,** *10* (7), 1274-81.

4. Scott-Taylor, T. H.; Axinia, S. C.; Amin, S.; Pettengell, R., Immunoglobulin G; structure and functional implications of different subclass modifications in initiation and resolution of allergy. *Immunity, inflammation and disease* **2018,** *6* (1), 13-33.

5. Kidd, P., Th1/Th2 balance: the hypothesis, its limitations, and implications for health and disease. *Altern Med Rev* **2003,** *8* (3), 223-46.

6. Rengarajan, J.; Szabo, S. J.; Glimcher, L. H., Transcriptional regulation of Th1/Th2 polarization. *Immunology Today* **2000,** *21* (10), 479-483.

7. Papa, I.; Vinuesa, C. G., Synaptic Interactions in Germinal Centers. *Front Immunol* **2018,** *9*, 1858.

8. Weisel, F. J.; Mullett, S. J.; Elsner, R. A.; Menk, A. V.; Trivedi, N.; Luo, W.; Wikenheiser, D.; Hawse, W. F.; Chikina, M.; Smita, S., Germinal center B cells selectively oxidize fatty acids for energy while conducting minimal glycolysis. *Nature immunology* **2020,** *21* (3), 331-342.

9. Martens, G. W.; Arikan, M. C.; Lee, J.; Ren, F.; Vallerskog, T.; Kornfeld, H., Hypercholesterolemia impairs immunity to tuberculosis. *Infection and immunity* **2008,** *76* (8), 3464-3472.

10. Narasimha, L.; Ponnusamy, T.; Philip, S.; Mukhopadhyay, R.; Kakkar, V.; Mundkur, L., Hypercholesterolemia Induced Immune Response and Inflammation on Progression of Atherosclerosis in Apob tm2Sgy Ldlr tm1Her/J Mice. *Lipids* **2015,** *50*.

11. Pollard, A. J.; Bijker, E. M., A guide to vaccinology: from basic principles to new developments. *Nat Rev Immunol* **2021,** *21* (2), 83-100.

12. Beatty, A. L.; Peyser, N. D.; Butcher, X. E.; Cocohoba, J. M.; Lin, F.; Olgin, J. E.; Pletcher, M. J.; Marcus, G. M., Analysis of COVID-19 Vaccine Type and Adverse Effects Following Vaccination. *JAMA Netw Open* **2021,** *4* (12), e2140364.

13. Wiedermann, U.; Garner-Spitzer, E.; Wagner, A., Primary vaccine failure to routine vaccines: Why and what to do? *Hum Vaccin Immunother* **2016,** *12* (1), 239-43.

14. Pellini, R.; Venuti, A.; Pimpinelli, F.; Abril, E.; Blandino, G.; Campo, F.; Conti, L.; De Virgilio, A.; De Marco, F.; Di Domenico, E. G.; Di Bella, O.; Di Martino, S.; Ensoli, F.; Giannarelli, D.; Mandoj, C.; Manciocco, V.; Marchesi, P.; Mazzola, F.; Moretto, S.; Petruzzi, G.; Petrone, F.; Pichi, B.; Pontone, M.; Zocchi, J.; Vidiri, A.; Vujovic, B.; Piaggio, G.; Morrone, A.; Ciliberto, G., Initial observations on age, gender, BMI and hypertension in antibody responses to SARS-CoV-2 BNT162b2 vaccine. *EClinicalMedicine* **2021,** *36*, 100928.

15. Makowski, L.; Chaib, M.; Rathmell, J. C., Immunometabolism: From basic mechanisms to translation. *Immunol Rev* **2020,** *295* (1), 5-14.

16. Weisel, F. J.; Mullett, S. J.; Elsner, R. A.; Menk, A. V.; Trivedi, N.; Luo, W.; Wikenheiser, D.; Hawse, W. F.; Chikina, M.; Smita, S.; Conter, L. J.; Joachim, S. M.; Wendell, S. G.; Jurczak, M. J.; Winkler, T. H.; Delgoffe, G. M.; Shlomchik, M. J., Germinal center B cells selectively oxidize fatty acids for energy while conducting minimal glycolysis. *Nat Immunol* **2020,** *21* (3), 331-342.

17. Zhou, X.; Zhu, X.; Zeng, H., Fatty acid metabolism in adaptive immunity. *FEBS J* **2021**.

18. Wang, A.; Luan, H. H.; Medzhitov, R., An evolutionary perspective on immunometabolism. *Science* **2019,** *363* (6423).

19. Bauby, H.; Ward, C. C.; Hugh-White, R.; Swanson, C. M.; Schulz, R.; Goujon, C.; Malim, M. H., HIV-1 Vpr Induces Widespread Transcriptomic Changes in CD4(+) T Cells Early Postinfection. *mBio* **2021,** *12* (3), e0136921.

20. Parnell, G.; McLean, A.; Booth, D.; Huang, S.; Nalos, M.; Tang, B., Aberrant cell cycle and apoptotic changes characterise severe influenza A infection--a meta-analysis of genomic signatures in circulating leukocytes. *PLoS One* **2011,** *6* (3), e17186.

21. Berdal, J. E.; Mollnes, T. E.; Waehre, T.; Olstad, O. K.; Halvorsen, B.; Ueland, T.; Laake, J. H.; Furuseth, M. T.; Maagaard, A.; Kjekshus, H.; Aukrust, P.; Jonassen, C. M., Excessive innate immune response and mutant D222G/N in severe A (H1N1) pandemic influenza. *The Journal of infection* **2011,** *63* (4), 308-16.

22. Kurupati, R.; Kossenkov, A.; Haut, L.; Kannan, S.; Xiang, Z.; Li, Y.; Doyle, S.; Liu, Q.; Schmader, K.; Showe, L.; Ertl, H., Race-related differences in antibody responses to the inactivated influenza vaccine are linked to distinct pre-vaccination gene expression profiles in blood. *Oncotarget* **2016,** *7* (39), 62898-62911.

23. Fischinger, S.; Boudreau, C. M.; Butler, A. L.; Streeck, H.; Alter, G., Sex differences in vaccine-induced humoral immunity. *Semin Immunopathol* **2019,** *41* (2), 239-249.

24. Voigt, E. A.; Ovsyannikova, I. G.; Kennedy, R. B.; Grill, D. E.; Goergen, K. M.; Schaid, D. J.; Poland, G. A., Sex Differences in Older Adults' Immune Responses to Seasonal Influenza Vaccination. *Front Immunol* **2019,** *10*, 180.

25. Braenne, I.; Kleinecke, M.; Reiz, B.; Graf, E.; Strom, T.; Wieland, T.; Fischer, M.; Kessler, T.; Hengstenberg, C.; Meitinger, T.; Erdmann, J.; Schunkert, H., Systematic analysis of variants related to familial hypercholesterolemia in families with premature myocardial infarction. *Eur J Hum Genet* **2016,** *24* (2), 191-7.

26. Fouchier, S. W.; Dallinga-Thie, G. M.; Meijers, J. C.; Zelcer, N.; Kastelein, J. J.; Defesche, J. C.; Hovingh, G. K., Mutations in STAP1 are associated with autosomal dominant hypercholesterolemia. *Circ Res* **2014,** *115* (6), 552-5.

27. Blanco-Vaca, F.; Martin-Campos, J. M.; Perez, A.; Fuentes-Prior, P., A rare STAP1 mutation incompletely associated with familial hypercholesterolemia. *Clin Chim Acta* **2018,** *487*, 270-274.

28. Sturm, A. C.; Knowles, J. W.; Gidding, S. S.; Ahmad, Z. S.; Ahmed, C. D.; Ballantyne, C. M.; Baum, S. J.; Bourbon, M.; Carrie, A.; Cuchel, M.; de Ferranti, S. D.; Defesche, J. C.; Freiberger, T.; Hershberger, R. E.; Hovingh, G. K.; Karayan, L.; Kastelein, J. J. P.; Kindt, I.; Lane, S. R.; Leigh, S. E.; Linton, M. F.; Mata, P.; Neal, W. A.; Nordestgaard, B. G.; Santos, R. D.; Harada-Shiba, M.; Sijbrands, E. J.; Stitziel, N. O.; Yamashita, S.; Wilemon, K. A.; Ledbetter, D. H.; Rader, D. J.; Convened by the Familial Hypercholesterolemia, F., Clinical Genetic Testing for Familial Hypercholesterolemia: JACC Scientific Expert Panel. *J Am Coll Cardiol* **2018,** *72* (6), 662-680.

29. Defesche, J. C.; Gidding, S. S.; Harada-Shiba, M.; Hegele, R. A.; Santos, R. D.; Wierzbicki, A. S., Familial hypercholesterolaemia. *Nature reviews. Disease primers* **2017,** *3*, 17093.

30. Di Taranto, M. D.; Giacobbe, C.; Fortunato, G., Familial hypercholesterolemia: A complex genetic disease with variable phenotypes. *European journal of medical genetics* **2020,** *63* (4), 103831.

31. Benito-Vicente, A.; Uribe, K. B.; Jebari, S.; Galicia-Garcia, U.; Ostolaza, H.; Martin, C., Familial Hypercholesterolemia: The Most Frequent Cholesterol Metabolism Disorder Caused Disease. *International journal of molecular sciences* **2018,** *19* (11).

32. Sniderman, A. D.; Tsimikas, S.; Fazio, S., The severe hypercholesterolemia phenotype: clinical diagnosis, management, and emerging therapies. *J Am Coll Cardiol* **2014,** *63* (19), 1935-47.

33. Karl, M.; Hasselwander, S.; Zhou, Y.; Reifenberg, G.; Kim, Y. O.; Park, K. S.; Ridder, D. A.; Wang, X.; Seidel, E.; Hovelmeyer, N.; Straub, B. K.; Li, H.; Schuppan, D.; Xia, N., Dual roles of B lymphocytes in mouse models of diet-induced nonalcoholic fatty liver disease. *Hepatology* **2022,** *76* (4), 1135-1149.

34. Mikhailova, S.; Ivanoshchuk, D.; Timoshchenko, O.; Shakhtshneider, E., Genes Potentially Associated with Familial Hypercholesterolemia. *Biomolecules* **2019,** *9* (12).

35. Yokohari, K.; Yamashita, Y.; Okada, S.; Ohya, K.; Oda, S.; Hatano, M.; Mano, H.; Hirasawa, H.; Tokuhisa, T., Isoform-dependent interaction of BRDG1 with Tec kinase. *Biochem Biophys Res Commun* **2001,** *289* (2), 414-20.

36. Ohya, K.; Kajigaya, S.; Kitanaka, A.; Yoshida, K.; Miyazato, A.; Yamashita, Y.; Yamanaka, T.; Ikeda, U.; Shimada, K.; Ozawa, K.; Mano, H., Molecular cloning of a docking protein, BRDG1, that acts downstream of the Tec tyrosine kinase. *Proc Natl Acad Sci U S A* **1999,** *96* (21), 11976-81.

37. Ferguson, D.; Finck, B. N., Emerging therapeutic approaches for the treatment of NAFLD and type 2 diabetes mellitus. *Nat Rev Endocrinol* **2021,** *17* (8), 484-495.

38. Masuhara, M.; Nagao, K.; Nishikawa, M.; Sasaki, M.; Yoshimura, A.; Osawa, M., Molecular cloning of murine STAP-1, the stem-cell-specific adaptor protein

containing PH and SH2 domains. *Biochem Biophys Res Commun* **2000,** *268* (3), 697-703.

39. Amor-Salamanca, A.; Castillo, S.; Gonzalez-Vioque, E.; Dominguez, F.; Quintana, L.; Lluis-Ganella, C.; Escudier, J. M.; Ortega, J.; Lara-Pezzi, E.; Alonso-Pulpon, L.; Garcia-Pavia, P., Genetically Confirmed Familial Hypercholesterolemia in Patients With Acute Coronary Syndrome. *J Am Coll Cardiol* **2017,** *70* (14), 1732-1740.

40. Cao, Y. X.; Wu, N. Q.; Sun, D.; Liu, H. H.; Jin, J. L.; Li, S.; Guo, Y. L.; Zhu, C. G.; Gao, Y.; Dong, Q. T.; Liu, G.; Dong, Q.; Li, J. J., Application of expanded genetic analysis in the diagnosis of familial hypercholesterolemia in patients with very early-onset coronary artery disease. *J Transl Med* **2018,** *16* (1), 345.

41. Danyel, M.; Ott, C. E.; Grenkowitz, T.; Salewsky, B.; Hicks, A. A.; Fuchsberger, C.; Steinhagen-Thiessen, E.; Bobbert, T.; Kassner, U.; Demuth, I., Evaluation of the role of STAP1 in Familial Hypercholesterolemia. *Sci Rep* **2019,** *9* (1), 11995.

42. Lamiquiz-Moneo, I.; Restrepo-Córdoba, M. A.; Mateo-Gallego, R.; Bea, A. M.; Del Pino Alberiche-Ruano, M.; García-Pavía, P.; Cenarro, A.; Martín, C.; Civeira, F.; Sánchez-Hernández, R. M., Predicted pathogenic mutations in STAP1 are not associated with clinically defined familial hypercholesterolemia. *Atherosclerosis* **2020,** *292*, 143-151.

43. Lamiquiz-Moneo, I.; Civeira, F.; Mateo-Gallego, R.; Laclaustra, M.; Moreno-Franco, B.; Tejedor, M. T.; Palacios, L.; Martin, C.; Cenarro, A., Diagnostic yield of sequencing familial hypercholesterolemia genes in individuals with primary hypercholesterolemia. *Rev Esp Cardiol (Engl Ed)* **2020**.

44. Loaiza, N.; Hartgers, M. L.; Reeskamp, L. F.; Balder, J. W.; Rimbert, A.; Bazioti, V.; Wolters, J. C.; Winkelmeijer, M.; Jansen, H. P. G.; Dallinga-Thie, G. M.; Volta, A.; Huijkman, N.; Smit, M.; Kloosterhuis, N.; Koster, M.; Svendsen, A. F.; van de Sluis, B.; Hovingh, G. K.; Grefhorst, A.; Kuivenhoven, J. A., Taking One Step Back in Familial Hypercholesterolemia: STAP1 Does Not Alter Plasma LDL (Low-Density Lipoprotein) Cholesterol in Mice and Humans. *Arterioscler Thromb Vasc Biol* **2020,** *40* (4), 973-985.

45. Kanuri, B.; Fong, V.; Haller, A.; Hui, D. Y.; Patel, S. B., Mice lacking global Stap1 expression do not manifest hypercholesterolemia. *BMC medical genetics* **2020,** *21* (1), 234.

46. https://www.ncbi.nlm.nih.gov/gene?Db=gene&Cmd=ShowDetailView&TermToSearch=7006.

47. Steeghs, E. M. P.; Bakker, M.; Hoogkamer, A. Q.; Boer, J. M.; Hartman, Q. J.; Stalpers, F.; Escherich, G.; de Haas, V.; de Groot-Kruseman, H. A.; Pieters, R.; den Boer, M. L., High STAP1 expression in DUX4-rearranged cases is not suitable as therapeutic target in pediatric B-cell precursor acute lymphoblastic leukemia. *Sci Rep* **2018,** *8* (1), 693.

48. Toda, J.; Ichii, M.; Oritani, K.; Shibayama, H.; Tanimura, A.; Saito, H.; Yokota, T.; Motooka, D.; Okuzaki, D.; Kitai, Y.; Muromoto, R.; Kashiwakura, J. I.; Matsuda, T.; Hosen, N.; Kanakura, Y., Signal-transducing adapter protein-1 is required for maintenance of leukemic stem cells in CML. *Oncogene* **2020,** *39* (34), 5601-5615.

49. Ishiura, M.; Kitai, Y.; Kashiwakura, J. I.; Muromoto, R.; Toda, J.; Ichii, M.; Oritani, K.; Matsuda, T., Positive interactions between STAP-1 and BCR-ABL influence chronic myeloid leukemia cell proliferation and survival. *Biochem Biophys Res Commun* **2021,** *556*, 185-191.

50. Lamiquiz-Moneo, I.; Restrepo-Cordoba, M. A.; Mateo-Gallego, R.; Bea, A. M.; Del Pino Alberiche-Ruano, M.; Garcia-Pavia, P.; Cenarro, A.; Martin, C.; Civeira, F.; Sanchez-Hernandez, R. M., Predicted pathogenic mutations in STAP1 are not associated with clinically defined familial hypercholesterolemia. *Atherosclerosis* **2020,** *292*, 143-151.

51. Amor-Salamanca, A.; Castillo, S.; Gonzalez-Vioque, E.; Dominguez, F.; Quintana, L.; Lluís-Ganella, C.; Escudier, J. M.; Ortega, J.; Lara-Pezzi, E.; Alonso-Pulpon, L.; Garcia-Pavia, P., Genetically Confirmed Familial Hypercholesterolemia in Patients With Acute Coronary Syndrome. *J Am Coll Cardiol* **2017,** *70* (14), 1732-1740.

52. Lamiquiz-Moneo, I.; Civeira, F.; Mateo-Gallego, R.; Laclaustra, M.; Moreno-Franco, B.; Tejedor, M. T.; Palacios, L.; Martin, C.; Cenarro, A., Diagnostic yield of sequencing familial hypercholesterolemia genes in individuals with primary hypercholesterolemia. *Rev Esp Cardiol (Engl Ed)* **2021,** *74* (8), 664-673.

53. Brænne, I.; Kleinecke, M.; Reiz, B.; Graf, E.; Strom, T.; Wieland, T.; Fischer, M.; Kessler, T.; Hengstenberg, C.; Meitinger, T.; Erdmann, J.; Schunkert, H.,

Systematic analysis of variants related to familial hypercholesterolemia in families with premature myocardial infarction. *Eur J Hum Genet* **2016,** *24* (2), 191-7.

54. Blanco-Vaca, F.; Martín-Campos, J. M.; Pérez, A.; Fuentes-Prior, P., A rare STAP1 mutation incompletely associated with familial hypercholesterolemia. *Clin Chim Acta* **2018,** *487*, 270-274.

55. Kashiwakura, J. I.; Saitoh, K.; Ihara, T.; Sasaki, Y.; Kagohashi, K.; Enohara, S.; Morioka, Y.; Watarai, H.; Muromoto, R.; Kitai, Y.; Iwabuchi, K.; Oritani, K.; Matsuda, T., Expression of signal-transducing adaptor protein-1 attenuates experimental autoimmune hepatitis via down-regulating activation and homeostasis of invariant natural killer T cells. *PloS one* **2020,** *15* (11), e0241440.

56. Saxena, A.; Chaudhary, U.; Bharadwaj, A.; Wahi, N.; Kalli, J. R.; Gupta, S.; Kumar, S.; Gupta, S.; Raj, U., A lung transcriptomic analysis for exploring host response in COVID-19. *J. Pure Appl. Microbiol* **2020**.

57. Doron, I.; Mesko, M.; Li, X. V.; Kusakabe, T.; Leonardi, I.; Shaw, D. G.; Fiers, W. D.; Lin, W. Y.; Bialt-DeCelie, M.; Roman, E.; Longman, R. S.; Pla, J.; Wilson, P. C.; Iliev, I. D., Mycobiota-induced IgA antibodies regulate fungal commensalism in the gut and are dysregulated in Crohn's disease. *Nat Microbiol* **2021,** *6* (12), 1493-1504.

58. Sun, J. B.; Holmgren, J.; Larena, M.; Terrinoni, M.; Fang, Y.; Bresnick, A. R.; Xiang, Z., Deficiency in Calcium-Binding Protein S100A4 Impairs the Adjuvant Action of Cholera Toxin. *Front Immunol* **2017,** *8*, 1119.

59. Sen Chaudhuri, A.; Yeh, Y. W.; Zewdie, O.; Li, N. S.; Sun, J. B.; Jin, T.; Wei, B.; Holmgren, J.; Xiang, Z., S100A4 exerts robust mucosal adjuvant activity for co-administered antigens in mice. *Mucosal Immunol* **2022,** *15* (5), 1028-1039.

60. Chen, W.; Patel, G. B.; Yan, H.; Zhang, J., Recent advances in the development of novel mucosal adjuvants and antigen delivery systems. *Hum Vaccin* **2010,** *6* (9).

61. Sanchez, J.; Holmgren, J., Cholera toxin - a foe & a friend. *Indian J Med Res* **2011,** *133* (2), 153-63.

62. Nelson, P. N.; Reynolds, G. M.; Waldron, E. E.; Ward, E.; Giannopoulos, K.; Murray, P. G., Monoclonal antibodies. *Mol Pathol* **2000,** *53* (3), 111-7.

63. Milstein, C., The hybridoma revolution: an offshoot of basic research. *Bioessays* **1999,** *21* (11), 966-73.

64. Tang, B. L., Glucose, glycolysis, and neurodegenerative diseases. *J Cell Physiol* **2020,** *235* (11), 7653-7662.

65. Presley, A. D.; Fuller, K. M.; Arriaga, E. A., MitoTracker Green labeling of mitochondrial proteins and their subsequent analysis by capillary electrophoresis with laser-induced fluorescence detection. *J Chromatogr B Analyt Technol Biomed Life Sci* **2003,** *793* (1), 141-50.

66. Xiao, B.; Deng, X.; Zhou, W.; Tan, E. K., Flow Cytometry-Based Assessment of Mitophagy Using MitoTracker. *Front Cell Neurosci* **2016,** *10*, 76.

67. Buckman, J. F.; Hernandez, H.; Kress, G. J.; Votyakova, T. V.; Pal, S.; Reynolds, I. J., MitoTracker labeling in primary neuronal and astrocytic cultures: influence of mitochondrial membrane potential and oxidants. *J Neurosci Methods* **2001,** *104* (2), 165-76.

68. Puleston, D., Detection of Mitochondrial Mass, Damage, and Reactive Oxygen Species by Flow Cytometry. *Cold Spring Harb Protoc* **2015,** *2015* (9), pdb prot086298.

69. Monteiro, L. B.; Davanzo, G. G.; de Aguiar, C. F.; Moraes-Vieira, P. M. M., Using flow cytometry for mitochondrial assays. *MethodsX* **2020,** *7*, 100938.

70. Murphy, M. P., How mitochondria produce reactive oxygen species. *Biochem J* **2009,** *417* (1), 1-13.

71. Kauffman, M. E.; Kauffman, M. K.; Traore, K.; Zhu, H.; Trush, M. A.; Jia, Z.; Li, Y. R., MitoSOX-Based Flow Cytometry for Detecting Mitochondrial ROS. *React Oxyg Species (Apex)* **2016,** *2* (5), 361-370.

72. Chen, Z.; Wang, J. H., How the Signaling Crosstalk of B Cell Receptor (BCR) and Co-Receptors Regulates Antibody Class Switch Recombination: A New Perspective of Checkpoints of BCR Signaling. *Front Immunol* **2021,** *12*, 663443.

73. Signorile, A.; Sgaramella, G.; Bellomo, F.; De Rasmo, D., Prohibitins: A Critical Role in Mitochondrial Functions and Implication in Diseases. *Cells* **2019,** *8* (1).

74. Bourges, I.; Ramus, C.; Mousson de Camaret, B.; Beugnot, R.; Remacle, C.; Cardol, P.; Hofhaus, G.; Issartel, J. P., Structural organization of mitochondrial human complex I: role of the ND4 and ND5 mitochondria-encoded subunits and interaction with prohibitin. *Biochem J* **2004,** *383* (Pt. 3), 491-9.

75. Wang, T.; Liu, H.; Itoh, K.; Oh, S.; Zhao, L.; Murata, D.; Sesaki, H.; Hartung, T.; Na, C. H.; Wang, J., C9orf72 regulates energy homeostasis by stabilizing mitochondrial complex I assembly. *Cell Metab* **2021,** *33* (3), 531-546 e9.

76. Tesfaye, D. Y.; Gudjonsson, A.; Bogen, B.; Fossum, E., Targeting Conventional Dendritic Cells to Fine-Tune Antibody Responses. *Front Immunol* **2019,** *10*, 1529.

77. Mellman, I., Dendritic cells: master regulators of the immune response. *Cancer Immunol Res* **2013,** *1* (3), 145-9.

78. Nazeri, S.; Zakeri, S.; Mehrizi, A. A.; Sardari, S.; Djadid, N. D., Measuring of IgG2c isotype instead of IgG2a in immunized C57BL/6 mice with Plasmodium vivax TRAP as a subunit vaccine candidate in order to correct interpretation of Th1 versus Th2 immune response. *Exp Parasitol* **2020,** *216*, 107944.

79. Aleebrahim-Dehkordi, E.; Molavi, B.; Mokhtari, M.; Deravi, N.; Fathi, M.; Fazel, T.; Mohebalizadeh, M.; Koochaki, P.; Shobeiri, P.; Hasanpour-Dehkordi, A., T helper type (Th1/Th2) responses to SARS-CoV-2 and influenza A (H1N1) virus: From cytokines produced to immune responses. *Transpl Immunol* **2022,** *70*, 101495.

80. Boothby, M. R.; Brookens, S. K.; Raybuck, A. L.; Cho, S. H., Supplying the trip to antibody production-nutrients, signaling, and the programming of cellular metabolism in the mature B lineage. *Cell Mol Immunol* **2022,** *19* (3), 352-369.

81. Liu, W.; Tolar, P.; Song, W.; Kim, T. J., Editorial: BCR Signaling and B Cell Activation. *Front Immunol* **2020,** *11*, 45.

82. Kitanaka, A.; Mano, H.; Conley, M. E.; Campana, D., Expression and activation of the nonreceptor tyrosine kinase Tec in human B cells. *Blood* **1998,** *91* (3), 940-8.

83. Ellmeier, W.; Jung, S.; Sunshine, M. J.; Hatam, F.; Xu, Y.; Baltimore, D.; Mano, H.; Littman, D. R., Severe B cell deficiency in mice lacking the tec kinase family members Tec and Btk. *J Exp Med* **2000,** *192* (11), 1611-24.

84. de Bruijn, M. J.; Rip, J.; van der Ploeg, E. K.; van Greuningen, L. W.; Ta, V. T.; Kil, L. P.; Langerak, A. W.; Rimmelzwaan, G. F.; Ellmeier, W.; Hendriks, R. W.;

Corneth, O. B., Distinct and Overlapping Functions of TEC Kinase and BTK in B Cell Receptor Signaling. *J Immunol* **2017,** *198* (8), 3058-3068.

85. Akkaya, M.; Traba, J.; Roesler, A. S.; Miozzo, P.; Akkaya, B.; Theall, B. P.; Sohn, H.; Pena, M.; Smelkinson, M.; Kabat, J.; Dahlstrom, E.; Dorward, D. W.; Skinner, J.; Sack, M. N.; Pierce, S. K., Second signals rescue B cells from activation-induced mitochondrial dysfunction and death. *Nature immunology* **2018,** *19* (8), 871-884.

86. Chueh, F. Y.; Leong, K. F.; Yu, C. L., Mitochondrial translocation of signal transducer and activator of transcription 5 (STAT5) in leukemic T cells and cytokine-stimulated cells. *Biochem Biophys Res Commun* **2010,** *402* (4), 778-83.

87. Zhang, L.; Zhang, J.; Liu, Y.; Zhang, P.; Nie, J.; Zhao, R.; Shi, Q.; Sun, H.; Jiao, D.; Chen, Y.; Zhao, X.; Huang, Y.; Li, Y.; Zhao, J. Y.; Xu, W.; Zhao, S. M.; Wang, C., Mitochondrial STAT5A promotes metabolic remodeling and the Warburg effect by inactivating the pyruvate dehydrogenase complex. *Cell Death Dis* **2021,** *12* (7), 634.

88. Hernando-Rodriguez, B.; Artal-Sanz, M., Mitochondrial Quality Control Mechanisms and the PHB (Prohibitin) Complex. *Cells* **2018,** *7* (12).

89. Belser, M.; Walker, D. W., Role of Prohibitins in Aging and Therapeutic Potential Against Age-Related Diseases. *Frontiers in genetics* **2021,** *12*, 714228.

90. Miwa, S.; Jow, H.; Baty, K.; Johnson, A.; Czapiewski, R.; Saretzki, G.; Treumann, A.; von Zglinicki, T., Low abundance of the matrix arm of complex I in mitochondria predicts longevity in mice. *Nature communications* **2014,** *5*, 3837.

91. Gupta, N.; DeFranco, A. L., Lipid rafts and B cell signaling. *Seminars in cell & developmental biology* **2007,** *18* (5), 616-26.

92. Maity, P. C.; Datta, M.; Nicolo, A.; Jumaa, H., Isotype Specific Assembly of B Cell Antigen Receptors and Synergism With Chemokine Receptor CXCR4. *Front Immunol* **2018,** *9*, 2988.

93. Mielenz, D.; Vettermann, C.; Hampel, M.; Lang, C.; Avramidou, A.; Karas, M.; Jack, H. M., Lipid rafts associate with intracellular B cell receptors and exhibit a B cell stage-specific protein composition. *J Immunol* **2005,** *174* (6), 3508-17.

94. Terashima, M.; Kim, K. M.; Adachi, T.; Nielsen, P. J.; Reth, M.; Kohler, G.; Lamers, M. C., The IgM antigen receptor of B lymphocytes is associated with prohibitin and a prohibitin-related protein. *The EMBO journal* **1994,** *13* (16), 3782-92.

95. Oyang, L.; Li, J.; Jiang, X.; Lin, J.; Xia, L.; Yang, L.; Tan, S.; Wu, N.; Han, Y.; Yang, Y.; Luo, X.; Li, J.; Liao, Q.; Shi, Y.; Zhou, Y., The function of prohibitins in mitochondria and the clinical potentials. *Cancer Cell Int* **2022,** *22* (1), 343.

96. Ontario, H., Genetic Testing for Familial Hypercholesterolemia: Health Technology Assessment. *Ont Health Technol Assess Ser* **2022,** *22* (3), 1-155.

97. Taghizadeh, E.; Taheri, F.; Gheibi Hayat, S. M.; Montecucco, F.; Carbone, F.; Rostami, D.; Montazeri, A.; Sahebkar, A., The atherogenic role of immune cells in familial hypercholesterolemia. *IUBMB Life* **2020,** *72* (4), 782-789.